약학박사 학위논문

Hybrid liposomes coated with amphiphilic hyaluronic acid derivative for targeted anticancer drug delivery and imaging

표적화된 항암제 전달 및 이미징을 위한

양친매성 히알루론산 유도체를 코팅한 하이브리드형 리포좀

2016년 2월

서울대학교 대학원

약학과 약제과학 전공

박 주 환

ABSTRACT

Hybrid liposomes coated with amphiphilic hyaluronic acid derivative for targeted anticancer drug delivery and imaging

Ju-Hwan Park

Department of Pharmaceutical Science

College of Pharmacy

The Graduate School

Seoul National University

Nanohybrid liposomes coated with amphiphilic hyaluronic acid–ceramide (HACE) was developed for targeted delivery of anticancer drug and *in vivo* cancer imaging. Doxorubicin (DOX) and Magnevist were used as a model anticancer drug and a magnetic resonance (MR) imaging probe, respectively. Nano-sized liposomal formulation which has mean diameter ranged from 120 to 130 nm and a narrow size distribution was developed. Encapsulation efficiency of DOX in liposomes was higher than 50%, and zeta potential of HACE-used liposomes (F3) was negatively higher than that of control liposomes (F2), indicating that liposomal surface was coated with

HACE. When the particle size distribution of both formulations was monitored in serum condition, HACE-coated liposomes showed enhanced stability than control liposomes, without forming aggregation. The prepared formulation showed sustained release profile and the release rate of DOX was increased in acidic pH than in physiological pH. *In vitro* cytotoxicity study, HACE-coated liposomes exhibited reduced cytotoxicity compared with control liposomes. In cellular uptake study, uptake of DOX from HACE-coated liposomes was improved by the interaction between HA and CD44 receptor. By MR imaging study, HACE-coated liposomes were demonstrated to have enhanced diagnostic activity with passive targeting and active targeting. In a pharmacokinetic study in rats, DOX encapsulated in liposomal formulation showed significantly prolonged circulation compared to DOX solution. In addition, pharmacokinetic parameters of liposomal formulation were further enhanced by surface coating with HACE, indicating that introducing HACE can increase *in vivo* stability. Based on these results, the HACE-coated nanoliposomal formulation may be a promising delivery system for targeted cancer therapy and cancer diagnosis.

Keywords: HACE; nanoliposomal formulation; tumor targeting; drug delivery; MR imaging; pharmacokinetic property

Student Number: 2012-30460

Contents

List of Tables

List of Figures

1. Introduction

1.1. Anticancer drugs

For the treatment of cancer, various types of anticancer drug have been developed for several decades. Each developed drug has its own mechanisms to cause cytotoxicity against cancer cells, including DNA-alkylation, DNA-crosslinking with organic heavy metal complex, topoisomerase inhibition, antimetabolites, and intercalation with DNA [1]. With these mechanisms, the drugs provoke apoptosis facilitation, metastasis inhibition, or angiogenesis inhibition, eventually treating cancer [2].

However, these anticancer drugs also have cytotoxicity against normal cells, thus they can cause unintended adverse effects. Because most of the anticancer drugs have low selectivity against tumor cells, unwanted accumulation of drug in normal tissues can be occurred, and this phenomenon can deteriorate cancer treatment. For example, doxorubicin, one of the anthracycline antibiotics, is reported to have a broad anticancer activity spectrum, so it can be used to treat various types of solid tumor [3, 4]. But the drug can cause cardiotoxicity and myelosuppression [5, 6]. Because of this dose-dependent toxicity and narrow therapeutic index, dose augmentation can be limited [7]. In another case, docetaxel, one of the most impactive anticancer agent over the past decade, shows cytotoxicity by blocking microtubules' function and inhibiting anti-apoptotic gene Bcl2 [8, 9]. With

these function, docetaxel has been used to treat many types of cancer, including breast cancer, non-small cell lung cancer, gastric adenocarcinoma, prostate cancer, and squamous cell cancer [10]. However, like other antitumor agents, these activities are not only aimed at tumor cells, but also at normal cells, thus the drug may raise haematologic side effects, thrombocytopenia, leukopenia, and anaemia, for example [10].

Except the adverse effects mentioned above, furthermore, the anticancer agents have other drawbacks, such as stability, solubility, and pharmacokinetic problems. For instance, camptothecin, a topoisomerase-targeting natural plant alkaloid, is reported to have a potent anticancer activity, but the drug has some limitations to be used in cancer treatment because of its poor water solubility and structural instability [11-13]. Camptothecin has an active lactone ring which can be rapidly hydrolyzed in bloodstream and become less active molecule [14, 15]. Meanwhile, doxorubicin, a potent anticancer agent explained above, shows very short distribution half-life and large volume of distribution when it is administered as a free form [16]. This rapid systemic distribution and short blood circulation can cause systemic toxicity and inefficient treatment.

1.2. Nanoparticulate delivery systems

As mentioned above, applying the anticancer drugs as an unfabricated form has numerous defects, leading to cancer treatment failure. To solve these problems, nanoparticulate carriers were introduced to drug delivery system.

There are various types of nano-sized drug delivery systems, including liposomes, polymeric micelles, solid lipid nanoparticles, nanoemulsion, dendrimers, and nanocomplexs. Diverse types of nanoparticulate drug delivery systems were developed, and these systems have gained much interests for cancer treatment [17-25].

Compared to unfabricated drug, nanoparticulate systems have numerous strong points. First, nanoparticles can encapsulate water-insoluble drugs. Hydrophobic drugs are hard to be absorbed orally, and easy to be precipitated when they are administered as a solution form. However, by incorporating the drugs to nanocarriers, drug solubilization problem can be solved. With this encapsulating property of nanoparticles, we can achieve sustained release drug delivery system. For the several decades, various methods were attempted to prepare sustained release system by using nanoparticle systems [26-29]. Especially, a biocompatible hydrophobic polymer, poly(lactic-co-glycolic) acid (PLGA), has been widely researched and usually showed very long-term release profiles over several weeks [30-33]. In addition, nanoparticle can enhance encapsulated drug's stability. It has been reported that some drugs unstable in the bloodstream can be protected by encapsulation into nanoparticle system [17, 34]. Moreover, pharmacokinetic properties can also be improved by nanocarriers. Normally, when hydrophilic drug is applied intravenously, it is rapidly eliminated by renal filtration [35]. And hydrophobic drug is usually transformed to hydrophilic metabolite by liver enzyme. In this case, nanoparticles can avoid uptake by reticuloendothelial (RES) system. If drug is encapsulated into nanoparticles, the drug can avoid

renal filtration and enzymatic metabolization, leading to prolonged blood circulation.

1.3. Tumor-targeting strategies

Above all, in anticancer drug delivery, tumor-targeting strategies can be granted via nanoparticle systems. Theoretically, tumor targeting mechanisms are normally classified into passive targeting and active targeting [36-38]. Between these strategies, passive tumor targeting is founded on enhanced permeability and retention (EPR) effect, and this effect is based on the nanoparticles' physical properties and peculiar characteristics of tumor region. Generally, it has been reported that tumor site has leaky vasculature condition and impaired lymphatic drainage system, unlike normal tissues or organs [39, 40]. In this condition, nanoparticles can selectively infiltrate into tumor region, without penetrating blood vessels of normal tissues. In addition, nanoparticles accumulated in tumor site are not easily eliminated because of the dysfunctional lymphatic system. Thus, anticancer agent-containing nanocarriers can be accumulated into tumor region and continuously show cytotoxicity by releasing the drug gradually.

Although the passive targeting strategy can contribute to the improved tumor targeted therapy, it also has some drawbacks. The mechanism has low tumor specificity, and cytotoxic potential to normal cells still exists. To complement this problem, diverse active targeting strategies have been tried by using tumor-tartgeting ligands, such as antibody, peptide, polysaccharide

and folic acid [41-43]. By conjugating tumor-targeting ligand with polymer, the polymer-based nanoparticles can be incorporated into tumor cells via receptor-mediated endocytosis. With this active targeting strategy, anticancer agents can be delivered to tumor region more selectively, resulting decrease of nonspecific cytotoxicity to normal cells.

1.4. Hyaluronic acid

Among the various ligands, hyaluronic acid (HA), a biocompatible polymer, has been widely researched as a tumor-targeting ligand for CD44 receptor which is overexpressed in several types of cancer cells [44-47]. Actually, other targeting ligands, including small molecules, peptides and proteins, should be conjugated to drugs or nanoparticle-composing polymers for the targeted anticancer drug delivery [48-50]. However, HA can form nano-sized formulations and deliver anticancer drugs to tumor site selectively by itself without conjugating other tumor-targeting ligands. Thus, HA can be a useful functional polymer which has large potential to be developed to tumor-targeting carrier systems.

Among the various nano-sized formulations, HA has been researched to prepare polymeric micelles by conjugating it with drug itself or other polymers, PLGA, alkyl chain, deoxycholic acid, for example [51-54]. Polymeric micelles are composed of amphiphilic polymer which has both hydrophilic group and hydrophobic group. When the polymer is dissolved in aqueous solvent at relatively high concentration, above the polymer's own

critical micelle concentration (CMC), it can form nano-sized micelles by self-assembling. With this fabrication, hydrophobic group forms core inside of micelles, and surface of the micelles is composed of polymer's hydrophilic group. In this case, poorly soluble drug can be encapsulated into the hydrophobic inner core and released by degrees.

In our previous studies, hyaluronic acid-ceramide (HACE) composed of hydrophilic hyaluronic acid oligomer and hydrophobic ceramide(CE) was synthesized and developed for targeted anticancer drug delivery (Fig.1) [55-58]. It was confirmed that HACE has proper amphiphilic property for the preparation of nano-sized micelles and CD44 receptor-mediated tumor targetability. In most researches, HACE showed sufficient anticancer drug encapsulation and sustained drug release profiles. In addition, the HA-based formulation did not show significant cytotoxicity against tested cells, indicating the nanocarrier's demonstrated safety. Above all, through in-depth investigations of the HACE nanoparticles using various cancer cell lines and animal models, the particle system was confirmed to have better antitumor efficacy and pharmacokinetic properties, compared to original anticancer agents. Furthermore, to overcome the own physicochemical defects of the HACE particles, other functional polymers were introduced to the delivery system by mixing or conjugation, and the research showed enhanced pharmaceutical properties [56-58].

1.5. Preliminary studies

With these excellent potentials mentioned above, HACE particulate system was modified or applied to other formulations. First, interconnecting HACE polymer was attempted for the further improvement of physicochemical characteristics of the HACE-based micelles [59]. Actually, the HACE nanoparticle system has superb tumor targetability and pharmacokinetic properties, but the delivery system still has some shortcomings such as somewhat low drug loading capacity, low *in vivo* stability, and insufficient drug release. *In vitro* release test of our previous study, only about 20% of drug was released from HACE nanoparticles for a week [55]. It is reported that surface or core crosslinking has been considered as a method for controlling drug release rate and in vivo pharmacokinetic performance [60-62]. For this purpose, by crosslinking each HACE molecule with adipic acid dihydrazide (ADH), interconnected HACE was prepared and researched for the enhanced anticancer drug delivery system (Fig.2). After the crosslinking, synthesis of interconnected HACE structure was confirmed by comparing interconnected polymer's ^{1}H-NMR spectrum with that of the unmodified HACE (Fig.3). The increase in the integration ratio of the chemical shifts at 1.5 ppm (-CH_2 of ADH and CE) to 0.9 ppm (terminal -CH_3 of CE) was indicative of the conjugated polymer. With the interconnected HACE, doxorubicin (DOX)-loaded polymeric micelles were prepared and their morphology was observed by transmission electron microscopy (TEM) (Fig.4b). Compared with unmodified HACE nanoparticles, interconnected HACE nanoparticles showed increased particle size, reduced zeta potential, and significantly increased DOX encapsulation efficiency (Table 1). The *in*

vitro release rate of interconnected HACE nanoparticles was higher than that of unmodified HACE nanoparticles, and both formulations did not induce serious cytotoxic effect (Fig.5 and Fig.6). *In vitro* cellular uptake study based on confocal laser scanning microscopy (CLSM), the fluorescence intensity of DOX in the interconnected HACE nanoparticles was slightly stronger than that of control HACE nanoparticles and DOX solution (Fig.7). Finally, *in vitro* antitumor efficacy test, DOX in the interconnected HACE nanoparticles eventually showed higher cytotoxic effect than the other two groups (Fig.8).

Meanwhile, HACE was combined with PLGA nanoparticle system for the preparation of new nano-sized carrier systems [63]. As mentioned above, PLGA, composed of lactic acid and glycolic acid, has suitable biocompatibility, biodegradability and sustained drug-releasing activity, so it was widely researched as a polymer for the various types of nanoparticle formulations, including anticancer drug delivery [30-33]. Although the PLGA has several advantages, the polymer's insufficient tumor targetabililty remains a limitation to be resolved. To improve PLGA nanoparticles' tumor targetability, many tumor targeting ligands have been introduced to the particle systems [64, 65]. To acquire the individual strong points of PLGA and HACE, embedding PLGA nanoparticles to self-assembled HACE nanostructure was attempted. As a result, docetaxel (DCT)-loaded nanoparticles which have narrow size distribution and spherical shape were prepared, and it was confirmed by particle size analyzer and scanning electron microscopy (SEM) (Fig.9). And compared to control PLGA nanoparticles, PLGA nanoparticle-embedded HACE nanostructure showed slightly increased

particle size and higher negative zeta potential (Table 2). By performing solid-state studies, including fourier-transform infrared (FT-IR) analysis, differential scanning calorimetry (DSC) analysis, and powder X-ray diffraction (PXRD) analysis, it was revealed that PLGA particles were incorporated into HACE nanostructure and DCT was encapsulated into nanoparticles as an amorphous form (Fig.10). *In vitro* DCT release test, sustained release patterns were observed for 10 days in both formulations (Fig.11). And both formulations did not showed significant cytotoxicity in the *in vitro* cytotoxicity test over the period tested (Fig.12). *In vitro* cellular uptake study observed by CLSM, the intensity of coumarin 6 loaded in each formulation was higher in HACE nanostructure group than in control PLGA nanoparticle group (Fig.13). Finally, through *in vivo* near-infrared fluorescence (NIRF) imaging study using tumor xenografted mouse model, it was confirmed that HACE nanostructure has better tumor targetability than control PLGA nanoparticles (Fig.14).

Through various experiments explained above, it was demonstrated that the development potential of HACE can be expanded. However, despite of modified formulations' enhanced physicochemical properties and tumor targetabilities, they are not perfectly applicable under *in vivo* condition. Especially, pharmacokinetic property was not improved yet in both cases [59, 63]. In addition, both formulations were not used to encapsulate probes for cancer diagnosis except a fluorescence probe.

1.6. Theranostics

Recently, a new pharmaceutical concept which combines disease diagnosis and drug delivery, so called "theranostics", has been researched for the excellent cancer therapy. The theranostic systems can provide efficient cancer treatment strategies and convenience for patients. Specifically, by applying the systems, we can deliver anticancer drugs to target site and grasp cancer prognosis simultaneously, thus optimized treatment plan can be selected. For this system, tumor-targeting strategies, generally consisting of passive and active targeting, have also been applied. By introducing suitable targeting techniques to theranostic systems, these techniques can maximize therapeutic efficacy and minimize side effects in the chemotherapy process. For these tumor-targeting-based strategies, nano-sized delivery systems have been widely researched. And related to cancer diagnosis, several probes for magnetic resonance (MR), positron emission tomography (PET), computed tomography (CT), single-photon emission computed tomography (SPECT), and fluorescence imaging have been introduced to the nano-sized delivery systems for the development of *in vivo* imaging techniques [57, 66, 67]. With these diagnostic probes, various formulations, including nanoparticles, micelles, liposomes, emulsions, and nanogels, have been used as carriers [56, 68-70].

1.7. Liposomes

Among the formulations above, liposomes have attracted much interest because of their advantages. Liposomes have biocompatibility and convenient size control property, and they can encapsulate both hydrophilic and hydrophobic drugs [71]. With these advantages, surface modification can be an appropriate way to enhance *in vivo* performance of liposomes. Related to this, surface-modification with hydrophilic polymers, such as polyethylene glycol, poly-N-vinyl pyrrolidone, polyvinyl alcohol, was used to improve the stability and circulation time of the liposomes in the blood stream [72-74]. It has been reported that the stability of a colloidal dispersion can be enhanced by the formation of protective shell composed of with hydrophilic polymers [71, 75]. In this regard, development of polymer hybridized liposomes can be a proper alternative for improving *in vivo* stability of original formulations.

In this investigation, HACE-coated nanohybrid liposomes were prepared for the targeted anticancer drug delivery MR imaging of cancer. As explained above, HACE has been used in tumor-targeted delivery of anticancer drugs [55, 56, 58]. In particular, HACE was also used to *in vivo* cancer imaging as a MR probe-conjugated form, but there was a complicated step to conjugate HACE polymer with MR imaging probes [57]. In this study, anticancer drug and MR imaging probe-encapsulated nanoliposomes were prepared by embedding amphiphilic HACE into the lipid bilayer of liposomal surface. To be specific, the hydrophobic residue (CE) may be anchored in the hydrophobic lipid bilayer and the hydrophilic chain (HA) attached to the outer surface of the liposomes (Fig.15). This combined formulation can acquire the advantages of both components; the tumor targetability of HACE and the *in*

vivo stability of the liposomes.

In this study, the physicochemical properties of the hybrid nanoliposomes, containing DOX and Magnevist, were investigated. And the formulation's cytotoxicity and cellular distribution were evaluated in MDA-MB-231 cells. Cancer diagnostic properties, by MR imaging, and *in vivo* pharmacokinetic properties of DOX were also assessed in animal models.

2. Materials and Methods

2.1. Materials

Doxorubicin hydrochloride (DOX HCl) was purchased from Boryung Pharmaceutical Co., Ltd. (Seoul, Korea). Egg phosphatidylcholine (Lipoid E100) was obtained from Lipoid AG (Ludwigshafen, Germany). Magnevist (N-methylglucamine salt of the gadolinium (Gd) complex of diethylenetriamine pentaacetic acid; gadopentetate dimeglumine) was purchased from Bayer HealthCare Pharmaceutical Inc. (Wayne, NJ, USA). HA oligomer and DS-Y30 (ceramide 3B; mainly N-oleoylphytosphingosine) were from Bioland Co., Ltd. (Cheonan, Korea) and Doosan Biotech Co., Ltd. (Yongin, Korea), respectively. Chloromethylbenzoyl chloride and tetra-n-butylammonium hydroxide (TBA) were obtained from Sigma-Aldrich Co. (St. Louis, MO, USA). Cell culture medium (RPMI 1640, Waymouth), penicillin,

streptomycin, N-2-hydroxyethylpiperazine-N-2-ethanesulfonic acid (HEPES) buffer solution, and heat-inactivated fetal bovine serum (FBS) were purchased from Gibco Life Technologies, Inc. (Grand Island, NY, USA). All other reagents were of analytical grade.

2.2. Preparation of DOX-loaded nanoliposomal formulations

HACE was synthesized as reported previously [58]. Briefly, HA (12.21 mmol) and TBA (9.77 mmol) were solubilized in double-distilled water (DDW; 60 mL) and stirred for 30 min. The resulting activated HA–TBA was acquired by freeze-drying. DS-Y30 ceramide (8.59 mmol) and triethylamine (9.45 mmol) in tetrahydrofuran (THF; 25 mL), and 4-chloromethylbenzoyl chloride (8.59 mmol) in THF (10 mL) were mixed to synthesize DS-Y30 linker. DS-Y30-containing linker was obtained from concentration and recrystallization processes after stirring for 6 h at 60 ℃. HA–TBA (8.10 mmol) and the DS-Y30-containing linker (0.41 mmol) were solubilized in THF/acetonitrile mixture (4:1, v/v) and stirred for 5 h at 40 ℃. After eliminating impurities and organic solvents, HACE was finally obtained.

The liposomal formulations were fabricated according to a reported liposome preparation method with minor modifications [76]. The composition of each formulation is presented in Table 3. Three formulations, Gd-loaded HACE-coated nanohybrid liposomes (F1), DOX/Gd-loaded liposomes (F2), and DOX/ Gd-loaded HACE-coated nanohybrid liposomes (F3) were prepared by a thin-film hydration method. For the preparation of F1

formulation, Lipoid E100 (80 mg), cholesterol (20 mg) and HACE (20 mg) were dissolved in methanol (20 mL) and the organic solvent was removed by evaporation (Büchi R-200 rotary evaporator, Flawil, Switzerland) at 60 ℃ for 30 min. After the evaporation, aqueous mixture containing Magnevist (2 mL) and 5 mM HEPES buffer (18 mL) was added to a thin film-coated flask and hydrated at 60 ℃ for 30 min. The resulting lipid dispersion was sonicated with a probe-type sonicator (Vibra-Cell VC 750 ultrasonic processor, Sonics & Materials, CT, USA) for 15 min, and passed through an extruder (Northern Lipids, Inc., Canada) equipped with 0.2 μm filter three times. For F2, Lipoid E100 (80 mg) and cholesterol (20 mg) were solubilized in methanol (20 mL) and the organic solvent was completely evaporated at 60 ℃ for 30 min. To remaining film, ammonium sulfate solution (250 mM, 10 mL) was added and hydrated at 60 ℃ for 30 min. Equal to F1, the resulting preparation was sonicated for 15 min and extruded three times. The liposomal dispersion was then blended with a mixture composed of DOX HCl (2 mg/mL) dissolved in 5 mM HEPES buffer (8 mL) and Magnevist (2 mL). For F3, HACE (20 mg) was added to the composition of F2 while other preparation methods were identical to that of F2. After preparing each formulation, it was incubated at 60 ℃ for 2 h. To remove unloaded salt, drug and Magnevist, the formulations were transferred into a dialysis bag (molecular weight cut-off: 6–8 kDa) and dialyzed against double-distilled water (DDW) for 2 days. For storage, 0.6 g of sucrose was dissolved to dialyzed dispersion and lyophilized.

2.3. Characterization of DOX-loaded liposomal formulations

The synthesis of HACE was characterized by ^{1}H-NMR as reported previously [58]. Characteristics of the nanoliposomal formulations, including particle size, polydispersity index, and zeta potential, were measured with a light-scattering spectrophotometer (ELS-Z; Otsuka Electronics, Tokyo, Japan). To compare the stability of liposomes in biological fluids, F2 and F3 formulations were incubated in PBS (pH 7.4) and 50% (v/v) FBS (in PBS, pH 7.4) for 1 or 24 h, and the mean particle size of each formulation was monitored. The encapsulation efficiency (EE) and DOX HCl content of each formulation were determined by high-performance liquid chromatography (HPLC) system after dispersing the formulations in DDW and diluting with 100× the volume of the mobile phase. The drug was assayed by Waters HPLC system (Waters Co., Milford, MA) equipped with a separation module (Waters e2695), a fluorescence detector (Waters 2475), and a reverse-phase C-18 column (Xbridge, RP-18, 250 × 4.6 mm, 5 μm; Waters Co.). For the quantification of DOX, fluorescence wavelengths of excitation and emission were set to 480 nm and 560 nm, respectively. The flow rate was 1.0 mL/min and the injection volume for analysis was 20 μL. The mobile phase consisted of 10 mM potassium phosphate buffer (pH 2.5) and acetonitrile containing 0.1% (w/w) triethylamine (71:29, v/v). The lower limit of quantification (LLOQ) was 25 ng/mL and precision and accuracy were within the acceptable range. Gd (major element of Magnevist) contents of each formulation were determined using an inductive coupled plasma-atomic emission spectrometer

(ICP–AES; Optima 4300 DV; PerkinElmer Inc., Wellesley, MA). The morphology of each liposomal formulation was observed by transmission electron microscopy (TEM). All formulations were adhered to Formvar/carbon-coated copper grids, stained with 2% uranyl acetate and washed with DDW. The liposome-adsorbed grids were then dried for 10 min and observed by TEM (JEM 1010; JEOL, Tokyo, Japan).

2.4. In vitro drug release test

DOX release test of F2 and F3 was performed *in vitro*. In this test, phosphate-buffered saline (PBS, pH 5.5, 6.8, and 7.4, adjusted with phosphoric acid) was used as a release media. The release pattern was monitored for 7 days at 37 ℃ with 50 r pm rotation using shaking bath. The formulation (equivalent to 50 μg DOX HCl) was added to a dialysis bag (molecular weight cut-off: 12-14 kDa) and was immersed in 20 mL of PBS (pH 5.5, 6.8, and 7.4). During the test, 0.2 mL PBS aliquot was collected and equal volume of fresh medium was replenished at predetermined time point (1, 3, 6, 9, 12, 24, 48, 72, 96, 120, 144, and 168 h). To analyze DOX concentration, HPLC system described above was used.

2.5. In vitro cytotoxicity test

MDA-MB-231 cells, human breast cancer cells, were obtained from the Korean Cell Line Bank (KCLB, Seoul, Korea). RPMI 1640 medium

containing 10% FBS, 100 U/mL penicillin, and 100 μg/mL streptomycin was used as a culturing medium, and the cells were cultured in CO_2 incubator (5% CO_2 atmosphere and 95% relative humidity at 37 ℃). The cytotoxicity of blank (with no loading DOX) F2 and F3 formulations was assessed by MTS-based assay. Cells were seeded in 96-well plates at a density of 1.0×10^4 per well, and incubated in CO_2 incubator for 24 h. After removing culture media, predetermined concentrations of blank F2 and F3 (0–500 μg/mL) were applied to cells and incubated for 24, 48, or 72 h under the same condition of cell culture. After the incubation, cells were treated with the MTS-based CellTiter 96 AQueous One Solution Cell Proliferation Assay Reagent (Promega Corp., WI, USA) at 37 ℃ for 4 h. Then, absorbance of each sample was detected at a wavelength of 490 nm with an EMax Precision Microplate Reader (Molecular Devices, Sunnyvale, CA, USA). With the absorbance data, cell viability (%) was calculated by comparison with the positive control (only culture media, without F2 or F3) on the same day.

2.6. In vitro cellular uptake study

Cellular uptake and distribution of the DOX in each formulation were evaluated in MDA-MB-231 cells by confocal laser scanning microscopy (CLSM). Cells were cultured based on the method described in cytotoxicity study section. For CLSM study, cells were seeded onto culture slides (surface area of 1.7 cm^2 per well, four-chamber slides, BD Falcon, Bedford, MA, USA) at a density of 1.0×10^5 per well, and incubated overnight in the CO_2

incubator. After removing cell culture media, DOX solution, F2, and F3 were added and incubated for 2 h. In this study, DOX concentration was set to 50 μg/mL. Next to the incubation, the cells were washed with PBS (pH 7.4) three times and fixed with 4% formaldehyde for 10 min. To prevent fading of fluorescence of DOX and to stain the nuclei, Vectashield mounting medium with 4′,6-diamidino-2-phenylindole (DAPI; H-1200; Vector Laboratories Inc., Burlingame, CA, USA) was used. Cellular uptake and distribution were then observed by CLSM (LSM 710; Carl-Zeiss, Thornwood, NY, USA).

2.7. Phantom study

MR images of prepared formulations (F1-F3) were acquired by 4.7-T MRI apparatus (BioSpec 47/40; Bruker, Karlsruhe, Germany). At 25-500 μM Gd, the T_1 contrast intensities of the prepared liposomes were scanned. The conditions for MRI were as follows: echo time (TE) = 7.76 ms, repetition time (TR) = 1000 ms, matrix = 128 × 128, field of view (FOV) = 5 × 6 cm, and slice thickness = 2 mm.

The T_1 relaxivity (r_1) was calculated using the following formula.

$$\left(\frac{1}{T_1}\right)_{obs} = \left(\frac{1}{T_1}\right)_{d} + r_1[\mathrm{M}]$$

In this equation, $(1/T_1)_{obs}$ and $(1/T_1)_{d}$ represents the relaxation rates of protons in the presence and absence of Gd, respectively, and [M] is the Gd concentration.

2.8. In vivo MRI study

The tumor targetability of nanoliposomes was confirmed by monitoring MR images of tumor-xenografted mice. To prepare MDA-MB-231 tumor-xenografted mouse model, female BALB/c nude mice (5 weeks old; Charles River, Wilmington, MA, USA) were used. An MDA-MB-231 cell suspension (2×10^6 cells in 0.1 mL culture medium) was subcutaneously injected into the right back of the mice. After tumor volume reaches $200mm^3$ (3 weeks post-injection), F2 and F3 were injected via the tail vein at a dose of 0.1 mmol Gd/kg. MR images of the cancer in the mouse model were obtained using a 4.7-T MRI apparatus (BioSpec 47/40; Bruker). T1-weighted images (axial section) were obtained before the injection and at 0, 30, 60, and 120 min post-injection. The conditions for the *in vivo* MRI study were as follows : TE = 10 ms, TR = 260 ms, FOV = 3.5 × 3.5 cm, matrix = 256 × 256, and slice thickness = 1 mm. The signal intensity (SI) in the region of interest (ROI), the tumor region, was calculated according to the reported method with slight modification [57]. Enhancement of the SI (%) is presented as the ratio between the increase in SI ($SI-SI_{pre}$) and the pre-image SI (SI_{pre}).

2.9. In vivo pharmacokinetic study

For the *in vivo* pharmacokinetic study of DOX, male Sprague Dawley rats (7–9 weeks old and weighing 200–250 g) were acquired from Orient Bio,

Inc. (Seongnam, South Korea). The animal study was approved by the Institutional Animal Care and Use Committee of Seoul National University (Seoul, Republic of Korea). Rats were maintained in a clean room (Animal Center for Pharmaceutical Research, College of Pharmacy, Seoul National University) at 20–23 ℃ and a relative humidity of 50 ± 5%. Drug administration and collecting blood samples were performed based on the reported method with minor modifications [56]. After anesthetizing rats, the femoral artery and vein of each rat were cannulated with a syringe-connected polyethylene tube (PE-50 ; Clay Adams, Parsippany, NJ). After the surgical operation, DOX solution, F2, and F3 were intravenously injected via the cannulated tube at a dose of 3 mg/kg. At predetermined times (1, 5, 15, 30, 45, 60, 90, and 120 min for DOX solution; 1, 5, 15, 30, 45, 60, 90, 120, 180, 240, 360, 540, and 1,440 min for F2 and F3), 300 μL of blood samples were collected via the cannulated femoral artery. After collecting each blood sample from rats, sodium chloride (0.9%) solution containing heparin (20 U/mL) was injected via the cannula immediately. After centrifuging blood samples, 150 μL of plasma was collected and stored at −70 ℃ until analysis. DOX in the plasma sample was analyzed by an HPLC method reported previously with slight modifications [56]. Each plasma sample (150 μL) was mixed with 10 μg/mL of propranolol HCl (internal standard) solution in DDW (25 μL) and acetonitrile (550 μL). After vortexing the mixture for 5 min and centrifuging (16 ,000 ×g, 5 min), 300 μL of supernatant was transferred to a new tube and the solvent was removed under a nitrogen gas stream at 50 ℃. After the evaporization, residues in the tubes were reconstituted with mobile

phase (60 μL) by vortexing for 5 min. Then all tubes were centrifuged (16,000 ×g, 5 min) and 10 μL of the clear supernatant was used for HPLC analysis. The composition of mobile phase used in the quantification of DOX in plasma was 10 mM potassium phosphate buffer (pH 2.5) and triethylamine-dissolved (0.1% (w/w) acetonitrile (73:27, v/v), and other analytical conditions were same as described method for the *in vitro* samples. The inter- and intra-day coefficients of variation were within the acceptable range. Pharmacokinetic parameters, such as total area under the plasma concentration–time curve from time zero to time infinity (AUC), terminal half-life ($t_{½}$), total body clearance (CL), apparent volume of distribution at steady state (V_{ss}), and mean residence time (MRT), were calculated using the WinNonlin software (Pharsight, Mountain View, CA, USA).

2.10. Data analysis

All experiments were performed at least three times and the data are expressed as means ± standard deviation (SD). Analysis of variance (ANOVA) was used for statistical analysis.

3. Results

3.1. Preparation and characterization of nanohybrid

liposomes

For the preparation of theranostic nanocarrier system, DOX HCl and Magnevist were used as a model drug and a MR imaging probe, respectively. And to grant active-tumor targeting moiety to liposomal system, HACE was introduced in liposome preparation process. In this investigation, we used HACE synthesized according to a reported method, and conjugation of the polymer was confirmed by ^{1}H-NMR analysis in a previous study [58]. And considering the lower ratio of HACE to lipid of nanoparticle formulation, F3 was expected to have polymer-hybridized liposomal structure. Because of this, a control HACE micellar group was omitted in this study. As a result of preparation, all formulations were generally homogeneous transparent. Through characterization of nanoliposomal formulations using particle size analyzer, it was confirmed that mean diameters of all formulations dispersed in DDW ranged from 120 to 130 nm (Table 4). A narrow-ranged size distribution of each formulation was confirmed by measuring polydispersity index and observing distribution histogram. In addition, the morphological shape of formulations was spherical as observed by TEM (Fig.16). And according to the data in Table 4, F2 and F3 liposomal formulations were confirmed to contain DOX with suitable encapsulation efficiency higher than 50%. Through this result, it was demonstrated that hydrophilic drug was successfully encapsulated by a remote loading method using an ammonium sulfate gradient. Meanwhile, not only the content of DOX, but the content of Magnevist was measured by quantification of Gd using ICP–AES. The

average values of Gd content (%) in lyophilized samples of F1, F2, and F3 were 3.56, 1.95, and 1.57%, respectively. And zeta potential of F3 was negatively higher than that of F2, indicating that surface of F3 was coated with negative HA part of HACE.

In addition to the basic characterization studies explained above, particle size monitoring test in biological fluid was also performed to compare the stability of each formulation *in vivo* condition. The particle size distribution of drug-loaded formulations (F2 and F3) dispersed in PBS or 50% FBS was monitored according to incubation time (Fig.17). The size distribution pattern of F2 and F3 in PBS was similar to that in DDW, without aggregation (Fig.17a). Despite the presence of salts in PBS, the liposomal formulations (F2 and F3) adequately maintained their stability. However, the size distribution pattern of the conventional liposomal formulation (F2) in 50% FBS was obviously altered. Aggregates larger than 1 μm were detected immediately after incubation in 50% FBS conditions (Fig.17b), and similar distribution pattern were observed after incubation for 1h and 24 h (Fig.17c and d). In contrast to the case of F2, HACE-coated formulation (F3) maintained the particle size distribution during the incubation time, exhibiting better stability *in vitro* of F3, compared with F2. These results support the prospect that F3 has superior *in vivo* stability and pharmacokinetic performance.

3.2. In vitro drug release test

DOX release pattern of F2 and F3 was monitored at pH 5.5, 6.8, and 7.4 (Fig.18). Overall, both formulations showed sustained release profile for 7 days and reached equilibrium at 6^{th} day in every pH condition. In each formulation group, release rate was increased in more acidic pH. In particular, after 7 days of release test, the released amounts of DOX from F3 were 30.45 ± 2.48% (pH 7.4), 42.88 ± 1.33% (pH 6.8), and 55.12 ± 1.84% (pH 5.5), respectively. Especially, the release amount of DOX from F3 was higher than that from F2 in pH 5.5, indicating that release rate can be enhanced after the endocytosis of liposomes to cancer cells. Interestingly, initial burst release pattern in F3 decreased at acidic condition compared to that in F2.

3.3. In vitro cytotoxicity test

In vitro Cytotoxicity of blank F2 and F3 formulations was evaluated using MDA-MB-231 cells. After incubating cells with various concentrations (up to 500 μg/mL) of blank formulations, cell viability (%) was measured by MTS-based assay after incubation for 24, 48, and 72 h (Fig.19). As a result, cell viability of F2 gradually decreased as time goes by. On the other hand, cell viability of F3 in all concentration range was almost 100% over the period tested (72 h). In particular, cell viabilities of F2- and F3- treated groups after incubation for 72 h were 40.67 ± 7.41 and 106.15 ± 1.92%, respectively. The results indicate that cytotoxicity of liposomes can be reduced by surface-coating with HACE.

3.4. In vitro cellular uptake study

The *in vitro* cellular distribution of DOX was estimated by CLSM after 2 h incubation of DOX samples. In this study, enhanced cellular uptake of HACE-coated liposomes was observed. With the distribution of DAPI (blue color), for the staining of nucleus, the intracellular distributions of DOX (red color) in DOX solution, F2, and F3 groups were captured in CLSM images (Fig.20). In DOX solution group, DOX was localized mainly in nucleus with a strong intensity. Compared to DOX solution group, the fluorescence intensity of control liposome group (F2) was weak. However, the intensity of DOX of F3 group was higher than that of F2 group and similar to that of solution group. According to these results, it was demonstrated that introducing HACE, tumor-targeting polymer, can enhance intracellular distribution of nanoliposomal formulation.

3.5. Phantom study

Because the MR imaging probe, Magnevist was encapsulated into the liposomal formulations, the diagnostic activity of the formulation should be assessed by *in vivo* MR imaging study. Prior to the study, phantom study was performed to measure each formulation's contrast-enhancing efficacy. In the Gd concentration range from 25 to 500 μM, the MR signal was enhanced as the concentration of Gd increased (Fig.21). T_1 relaxivity (r_1) values of F1, F2, and F3, calculated by the equation described in the section 2.7., were 5.94,

6.29, and 6.35 mM^{-1} s^{-1}, respectively. From the results, the linearity was established between Gd concentration and the $1/T_1$ value.

3.6. In vivo MRI study

The *in vivo* diagnostic capabilities of the nanoliposomal formulations (F2 and F3) were evaluated using a MDA-MB-231 tumor-xenografted mouse model. In this study, after the intravenous injection of F2 and F3 to the tumor-xenografted mice, T_1-weighed MR images of the mice were obtained at predetermined time points (Fig.22). Because Magnevist was reported to be nonspecifically distributed and rapidly eliminated from the body, MR images of the Magnevist itself were not acquired in this experiment [77]. When the contrast enhancing effect of each formulation in tumor region was quantified, the enhancement of SI value for F2 ranged from 31.12 to 37.92% for 2 h, while the SI value for F3 was increased up to 89.12% at 2 h post-injection (Fig.23). The SI enhancement of F3 at 2 h was 2.59-fold higher than that of F2. According to these results, it was seemed that F3 was accumulated to tumor region with better intensity than F2 by additional active targeting activity based on interaction between HA and CD44 receptor.

3.7. In vivo pharmacokinetic study

The *in vivo* pharmacokinetic properties of DOX after intravenous administration in rats were investigated. DOX concentrations in the plasma-

time profiles of DOX solution, F2, and F3 are presented and pharmacokinetic parameters calculated from the drug concentration-time profiles are also shown (Fig.24 and Table 5). Compared to CL of DOX solution group (67.97 ± 9.01 mL/min/kg), the CL value of F2 and F3 was decreased to 0.57 ± 0.16 mL/min/kg and 0.22 ± 0.06 mL/min/kg, respectively. And AUC values of F2 (5491.31 ± 1226.13 μg min/mL) and F3 (14731.33 ± 3793.55 μg min/mL) were increased significantly ($P < 0.05$), compared with that of DOX solution (44.86 ± 6.84 μg min/mL). In addition, terminal $t_{½}$ and MRT of F2 and F3 were also clearly increased versus the DOX solution ($P < 0.05$). The V_{ss} values of F2 and F3 were also significantly lower than that of DOX solution ($P < 0.05$). In addition to the obvious alterations in pharmacokinetic parameters of the both formulations (F2 and F3) versus DOX solution, there were also significant differences in the pharmacokinetic parameters between F2 and F3. According to the pharmacokinetic parameter data, *in vivo* clearance (CL) of F3 was decreased to 38.60% of CL for F2 ($P < 0.05$). AUC, terminal $t_{½}$, and MRT values of F3 were 2.68-, 1.52-, and 1.61-fold higher than those of F2, respectively. These results indicate that F3 shows a prolonged circulation property, resulting enhanced pharmacokinetic performance, compared to DOX solution and F2.

4. Discussion

In this study, HACE-coated hybrid nanoliposomes were prepared for the

targeted drug delivery and enhanced MR imaging of cancer. A synthesized amphiphilic polymer, HACE was introduced to conventional liposomal formulation for the fabrication of tumor-targetable nanocarrier system. As mentioned above, HA has been widely used to the targeted drug delivery system and cancer diagnosis because of its targeting ability for CD44 receptor-overexpressing tumor cells. In our previous studies, HACE was successfully used for the tumor-targeted drug delivery and cancer imaging [55-58]. In these former studies, HACE formed nano-sized micelles and encapsulated hydrophobic drug by its self-assembling properties. HACE has tumor-targetability and self-assembly as explained above, and liposomal formulation can encapsulate hydrophilic drug and has superior *in-vivo* stability. To gain the merits of both formulations, nanoliposomal formulation coated with HACE was prepared. As described above and in Fig.15, considering the chemical structures of HACE and phospholipid, a material of liposomes, it is estimated that CE residue of HACE is embedded in the lipid bilayer and the hydrophilic surface of the liposomes is coated with HA part.

An anticancer agent, DOX HCl was encapsulated into the nanoliposomal formulations, and Magnevist was also incorporated into the hydrophilic core of them. To encapsulate DOX efficiently, remote loading method with ammonium sulfate gradient was used. During the preparation of formulation, the concentration of ammonium sulfate in the core of the liposome is higher than that of the external aqueous phase. This condition makes DOX be accumulated to the inner core. Then the weak base, DOX forms gel-like precipitate with negative charged sulfate ion [78, 79]. With these mechanisms,

DOX can be encapsulated into the liposomal formulation with a high efficiency.

After the preparation, all formulations showed particle size ranged from 120 to 130 nm and narrow size distribution. Although the measured particle size is suitable for the passive targeting strategy based on EPR effect, monitoring particle size in the blood stream is considered to be more important for the *in vivo* intravenous application of formulation. It has been reported that intravenously administered nanoparticles can interact with various biological components in the blood stream and form large aggregates [80, 81]. By this phenomenon, blood circulation of nanoparticles can shorten, and the aggregates can be accumulated into unwanted organs. Because of these reasons, the stability of nanoliposomal formulations should be evaluated in biological fluids. As shown in Fig.17, HACE-coated F3 showed better stability in the presence of serum compared to F2. These results represent F3 can perform improved *in vivo* circulation and diagnostic accuracy based on its superior *in vivo* stability.

In vitro release test, release rate of DOX was faster in more acidic pH condition, and this profile was shown in both formulations. These results can be explained by the increase of DOX solubility in acidic pH and weakening of interactions between DOX and liposomal formulation. Higher DOX release in acidic pH conditions can be helpful in anticancer drug delivery. The pH of tumor regions is more acidic than that of normal organs, and this may improve anti-tumor efficacy in tumor site and decrease toxicity in normal regions. Meanwhile, lower burst release pattern was detected in F3, compared to F2.

As shown in Table 4, zeta potential of F2 is less negative than that of F1, due to part of DOX being adsorbed on the liposomal surface with charge interaction. From the data, it is estimated that the interaction between DOX and HACE can retard the initial drug release.

In vitro cytotoxicity test, F3 showed significant less cytotoxicity against MDA-MB-231 cells than F2. In this test, F2 dispersion applied to cells formed aggregation in high concentration range during incubation time, and this precipitates caused cytotoxicity. However, F3 did not showed aggregation in all concentration range, resulting cell viability around 100%. This appearance is similar to the result of the stability test in biological fluids (Fig.17). The cytotoxicity of the liposomal formulations is dependent on several factors, including the lipid type, the amount of lipid, and the charge of the lipid [82, 83]. In the case of F3, HACE coated on the outer surface of liposomal formulation seems to have prevented the disruption of cellular membranes caused by lipid. In addition, HACE granted negative charge to the liposomal surface, and this may inhibit aggregation of nanoliposomes. The low cytotoxicity of the HACE-liposome (F3), compared with the plain liposomal formulation (F2), will enhance the safety of the nanocarrier itself, facilitating its successful use in *in vivo* condition.

MDA-MB-231 cell, used to evaluate the nanoliposomal formulations is a human breast cancer cell line that overexpresses the CD44 receptor, so the cell line was used in the research of the interaction between HA and CD44 receptor [84]. In the *in vitro* cellular uptake test, F3 showed improved cellular uptake to MDA-MB-231 cells compared to F2, and the uptake DOX intensity

of F3 was similar to that of solution form. In the case of DOX solution, DOX can penetrate cell membrane by diffusion, so relatively large amount of drug can freely enter the cancer cells and become localized in cell nucleus. On the other hand, in the case of F2, DOX is incorporated in liposomal formulation which has no targeting moiety. Because of sustained release property of the liposomal formulation, less amount of DOX diffuse to tumor cells from the extracellular space, leading to less cellular uptake. However, F3 has active targeting moiety, so the formulation can enter the cells with higher intensity via receptor-mediated endocytosis (RME). In our previous research, HACE nanoparticles were demonstrated to have uptake mechanism based on RME pathway [55-58]. Considering this active targeting of the HACE and the result of *in vitro* cellular uptake test, F3 is expected to perform superior targeted drug delivery to tumor site, compared to normal liposomal formulation.

For the efficient cancer diagnosis, various strategies using MR imaging have been researched. Through phantom study, all formulation (F1, F2 and F3) exhibited similar contrast-enhancing efficacy and linearity between the enhancing effect and Gd concentration. With these diagnostic activities, in vivo MR imaging performance of each formulation was evaluated using tumor-xenografted nude mouse model. As shown in Fig.22 and Fig.23, it was confirmed that the larger amount of Magnevist loaded in F3 was accumulated in tumor region than that of F2. Of course, F2 is also a nano-sized system, so the formulation can be distributed to tumor site by passive targeting strategy based on EPR effect. However, F3 can target tumor region more actively than F2, via HA-CD44 receptor interaction, resulting improved contrast-enhancing

effect. The tendency of these results is similar to *in vitro* cellular uptake study (Fig.20) and our previous reports [56-58]. In addition, the stability data in biological fluids shown in Fig.17 also support the diagnostic excellence of HACE-used formulation. It can be estimated that enhanced stability of nanoliposomal formulation in bloodstream contributed to avoidance of RES system and efficient MR probe delivery to tumor region. Considering these supporting data, we can conclude that the HACE-coated nanoliposomal formulation can perform both drug delivery and cancer diagnosis with an adequate tumor targeting and stability.

Finally, in the *in vivo* pharmacokinetic study, both liposomal formulations (F2 and F3) showed significantly prolonged drug circulation profile compared to DOX solution. By encapsulating DOX into liposomes, AUC, $t_{½}$ and MRT were increased, and CL and V_{ss} were decreased. And between both liposomal formulations, pharmacokinetic parameters of F3 were improved than those of F2. Because DOX has low molecular weight and amphiphilicity, free DOX can be rapidly distributed to tissues and organs systemically. In the *in vitro* cellular uptake test, the large amount of DOX solution permeated into the cancer cells. However, under *in vivo* condition, free DOX is rapidly eliminated from the central compartment of body, so it could not be delivered to tumor region intensively. Moreover, nonspecifically distributed DOX can cause serious adverse effects to normal tissues and organs. In contrast to solution form, liposomal formulations are usually restricted to the central compartment, and this phenomenon leads to the decrease of V_{ss} [85, 86]. By inhibiting rapid distribution of drug and sustained

release property, liposomes can prolong the circulation time of the drug. Meanwhile, compared to F2, enhanced pharmacokinetic parameters of F3 could be explained by its stability in biological fluids. As described in Fig.17, F2 formulations formed aggregation in serum condition, but F3 did not. HACE coating of liposomes may contribute to the reduction of the interaction with serum opsonins and uptake by RES, resulting prolonged circulation of liposomes in the blood stream. Thus, we can confirm that HACE coating can not only enhance diagnostic efficiency of nanocarrier system but can prolong the circulation time of applied formulations.

5. Conclusion

For the targeted anticancer drug delivery and MR imaging of cancer, HACE-coated nanoybrid liposomal formulation was developed and evaluated. As a result of preparation, nano-sized liposomes around 120 nm with narrow size distribution were prepared. The prepared formulation showed sustained DOX release pattern, and the release rate was increased at acidic pH. Compared to F2, HACE-used F3 showed excellent serum stability and lower *in vitro* cellular cytotoxicity. And because of the active targeting moiety of F3, cellular uptake of DOX from the F3 was higher than that from F2. By *in vivo* MR imaging study, diagnostic efficiency of both formulations were compared, and F3 was confirmed to have superior contrast-enhancing effect than F2 with higher tumor selectivity. Furthermore, HACE-coating enhanced *in vivo*

stability of liposomal formulation, resulting prolongation of drug circulation time and improvement of pharmacokinetic parameters. According to the data explained above, the developed HACE-coated nanoliposomal formulation is considered to a promising delivery system for the targeted anticancer agent delivery and precise tumor imaging.

6. References

1. PAYNE, S. and D. MILES, *Mechanisms of anticancer drugs.* Basic Clinical Radiobiology, 2016: p. 134.
2. Narang, A.S., D. Desai, Y. Lu, and R. Mahato, *Unique aspects of pharmaceutical development.* Anticancer drug development, 2009: p. 49-92.
3. Carter, S., *ADRIAMYCIN (NSC-123127)-THOUGHTS FOR FUTURE.* CANCER CHEMOTHERAPY REPORTS PART 3 PROGRAM INFORMATION-SUPPLEMENT, 1975. **6**(2): p. 389-397.
4. Young, R.C., R.F. Ozols, and C.E. Myers, *The anthracycline antineoplastic drugs.* New England Journal of Medicine, 1981. **305**(3): p. 139-153.
5. Bally, M.B., R. Nayar, D. Masin, P.R. Cullis, and L.D. Mayer, *Studies on the myelosuppressive activity of doxorubicin entrapped in liposomes.* Cancer Chemother Pharmacol, 1990. **27**(1): p. 13-9.
6. Rahman, A., A. Joher, and J.R. Neefe, *Immunotoxicity of multiple dosing regimens of free doxorubicin and doxorubicin entrapped in cardiolipin liposomes.* Br J Cancer, 1986. **54**(3): p. 401-8.
7. Mitra, S., U. Gaur, P.C. Ghosh, and A.N. Maitra, *Tumour targeted delivery of encapsulated dextran-doxorubicin conjugate using chitosan nanoparticles as carrier.* J Control Release, 2001. **74**(1-3): p. 317-23.
8. Shelley, M., C. Harrison, B. Coles, J. Staffurth, T.J. Wilt, and M.D.

Mason, *Chemotherapy for hormone-refractory prostate cancer.* Cochrane Database Syst Rev, 2006. **4**.

9. Van Poppel, H., *Recent docetaxel studies establish a new standard of care in hormone refractory prostate cancer.* Can J Urol, 2005. **12 Suppl 1**: p. 81-5.

10. Baker, J., J. Ajani, F. Scotte, D. Winther, M. Martin, M.S. Aapro, and G. von Minckwitz, *Docetaxel-related side effects and their management.* Eur J Oncol Nurs, 2009. **13**(1): p. 49-59.

11. Hsiang, Y.H. and L.F. Liu, *Identification of mammalian DNA topoisomerase I as an intracellular target of the anticancer drug camptothecin.* Cancer Res, 1988. **48**(7): p. 1722-6.

12. Me, W. and C. Cook, *The isolation and structure of camptothecin, a novel alkaloidal leukemia and tumor.* J Am Chem Soc, 1966. **88**(16): p. 3888-3890.

13. Potmesil, M., *Camptothecins: from bench research to hospital wards.* Cancer Res, 1994. **54**(6): p. 1431-9.

14. Fassberg, J. and V.J. Stella, *A kinetic and mechanistic study of the hydrolysis of camptothecin and some analogues.* J Pharm Sci, 1992. **81**(7): p. 676-84.

15. Akimoto, K., A. Kawai, and K. Ohya, *Kinetic Studies of the Hydrolysis and Lactonization of Camptothecin and Its Derivatives, CPT-11 and SN-38, in Aqueous Solution.* Chemical and pharmaceutical bulletin, 1994. **42**(10): p. 2135-2138.

16. Rahman, A., D. Carmichael, M. Harris, and J.K. Roh, *Comparative*

pharmacokinetics of free doxorubicin and doxorubicin entrapped in cardiolipin liposomes. Cancer Res, 1986. **46**(5): p. 2295-9.

17. Min, K.H., K. Park, Y.S. Kim, S.M. Bae, S. Lee, H.G. Jo, R.W. Park, I.S. Kim, S.Y. Jeong, K. Kim, and I.C. Kwon, *Hydrophobically modified glycol chitosan nanoparticles-encapsulated camptothecin enhance the drug stability and tumor targeting in cancer therapy.* J Control Release, 2008. **127**(3): p. 208-18.

18. Kolishetti, N., S. Dhar, P.M. Valencia, L.Q. Lin, R. Karnik, S.J. Lippard, R. Langer, and O.C. Farokhzad, *Engineering of self-assembled nanoparticle platform for precisely controlled combination drug therapy.* Proc Natl Acad Sci U S A, 2010. **107**(42): p. 17939-44.

19. Cho, H. and G.S. Kwon, *Polymeric micelles for neoadjuvant cancer therapy and tumor-primed optical imaging.* ACS Nano, 2011. **5**(11): p. 8721-9.

20. Koo, H., S. Lee, J.H. Na, S.H. Kim, S.K. Hahn, K. Choi, I.C. Kwon, S.Y. Jeong, and K. Kim, *Bioorthogonal copper-free click chemistry in vivo for tumor-targeted delivery of nanoparticles.* Angew Chem Int Ed Engl, 2012. **51**(47): p. 11836-40.

21. Termsarasab, U., H.J. Cho, D.H. Kim, S. Chong, S.J. Chung, C.K. Shim, H.T. Moon, and D.D. Kim, *Chitosan oligosaccharide-arachidic acid-based nanoparticles for anti-cancer drug delivery.* Int J Pharm, 2013. **441**(1-2): p. 373-80.

22. Termsarasab, U., H.J. Cho, H.T. Moon, J.H. Park, I.S. Yoon, and D.D. Kim, *Self-assembled magnetic resonance imaging nanoprobes based*

on arachidyl chitosan for cancer diagnosis. Colloids Surf B Biointerfaces, 2013. **109**: p. 280-6.

23. Yoon, G., J.W. Park, and I.-S. Yoon, *Solid lipid nanoparticles (SLNs) and nanostructured lipid carriers (NLCs): recent advances in drug delivery.* Journal of Pharmaceutical Investigation, 2013. **43**(5): p. 353-362.

24. Yoon, H.Y., H. Koo, K.Y. Choi, I. Chan Kwon, K. Choi, J.H. Park, and K. Kim, *Photo-crosslinked hyaluronic acid nanoparticles with improved stability for in vivo tumor-targeted drug delivery.* Biomaterials, 2013. **34**(21): p. 5273-80.

25. Zhang, R., K. Luo, J. Yang, M. Sima, Y. Sun, M.M. Janat-Amsbury, and J. Kopecek, *Synthesis and evaluation of a backbone biodegradable multiblock HPMA copolymer nanocarrier for the systemic delivery of paclitaxel.* J Control Release, 2013. **166**(1): p. 66-74.

26. Stover, T.C., Y.S. Kim, T.L. Lowe, and M. Kester, *Thermoresponsive and biodegradable linear-dendritic nanoparticles for targeted and sustained release of a pro-apoptotic drug.* Biomaterials, 2008. **29**(3): p. 359-69.

27. Chavanpatil, M.D., A. Khdair, Y. Patil, H. Handa, G. Mao, and J. Panyam, *Polymer-surfactant nanoparticles for sustained release of water-soluble drugs.* J Pharm Sci, 2007. **96**(12): p. 3379-89.

28. Hindi, K.M., A.J. Ditto, M.J. Panzner, D.A. Medvetz, D.S. Han, C.E. Hovis, J.K. Hilliard, J.B. Taylor, Y.H. Yun, C.L. Cannon, and W.J.

Youngs, *The antimicrobial efficacy of sustained release silver-carbene complex-loaded L-tyrosine polyphosphate nanoparticles: characterization, in vitro and in vivo studies.* Biomaterials, 2009. **30**(22): p. 3771-9.

29. Tasset, C., N. Barette, S. Thysman, J.-M. Ketelslegers, D. Lemoine, and V. Pre, *Polyisobutylcyanoacrylate nanoparticles as sustained release system for calcitonin.* Journal of controlled release, 1995. **33**(1): p. 23-30.

30. Yoo, H.S., J.E. Oh, K.H. Lee, and T.G. Park, *Biodegradable nanoparticles containing doxorubicin-PLGA conjugate for sustained release.* Pharm Res, 1999. **16**(7): p. 1114-8.

31. Yoo, H.S., K.H. Lee, J.E. Oh, and T.G. Park, *In vitro and in vivo anti-tumor activities of nanoparticles based on doxorubicin-PLGA conjugates.* J Control Release, 2000. **68**(3): p. 419-31.

32. Mu, L. and S.S. Feng, *A novel controlled release formulation for the anticancer drug paclitaxel (Taxol): PLGA nanoparticles containing vitamin E TPGS.* J Control Release, 2003. **86**(1): p. 33-48.

33. Avgoustakis, K., A. Beletsi, Z. Panagi, P. Klepetsanis, A.G. Karydas, and D.S. Ithakissios, *PLGA-mPEG nanoparticles of cisplatin: in vitro nanoparticle degradation, in vitro drug release and in vivo drug residence in blood properties.* J Control Release, 2002. **79**(1-3): p. 123-35.

34. Díaz, M.R. and P.E. Vivas-Mejia, *Nanoparticles as drug delivery systems in cancer medicine: emphasis on RNAi-containing*

nanoliposomes. Pharmaceuticals, 2013. **6**(11): p. 1361-1380.

35. Li, S.-D. and L. Huang, *Pharmacokinetics and biodistribution of nanoparticles.* Molecular pharmaceutics, 2008. **5**(4): p. 496-504.

36. Danhier, F., O. Feron, and V. Preat, *To exploit the tumor microenvironment: Passive and active tumor targeting of nanocarriers for anti-cancer drug delivery.* J Control Release, 2010. **148**(2): p. 135-46.

37. Lammers, T., F. Kiessling, W.E. Hennink, and G. Storm, *Drug targeting to tumors: principles, pitfalls and (pre-) clinical progress.* J Control Release, 2012. **161**(2): p. 175-87.

38. Maeda, H., H. Nakamura, and J. Fang, *The EPR effect for macromolecular drug delivery to solid tumors: Improvement of tumor uptake, lowering of systemic toxicity, and distinct tumor imaging in vivo.* Adv Drug Deliv Rev, 2013. **65**(1): p. 71-9.

39. Maeda, H., J. Fang, T. Inutsuka, and Y. Kitamoto, *Vascular permeability enhancement in solid tumor: various factors, mechanisms involved and its implications.* Int Immunopharmacol, 2003. **3**(3): p. 319-28.

40. Matsumura, Y. and H. Maeda, *A new concept for macromolecular therapeutics in cancer chemotherapy: mechanism of tumoritropic accumulation of proteins and the antitumor agent smancs.* Cancer Res, 1986. **46**(12 Pt 1): p. 6387-92.

41. Zhong, Y., F. Meng, C. Deng, and Z. Zhong, *Ligand-directed active tumor-targeting polymeric nanoparticles for cancer chemotherapy.*

Biomacromolecules, 2014. **15**(6): p. 1955-69.

42. Danhier, F., E. Ansorena, J.M. Silva, R. Coco, A. Le Breton, and V. Preat, *PLGA-based nanoparticles: an overview of biomedical applications.* J Control Release, 2012. **161**(2): p. 505-22.

43. Kamaly, N., Z. Xiao, P.M. Valencia, A.F. Radovic-Moreno, and O.C. Farokhzad, *Targeted polymeric therapeutic nanoparticles: design, development and clinical translation.* Chemical Society Reviews, 2012. **41**(7): p. 2971-3010.

44. Culty, M., M. Shizari, E.W. Thompson, and C.B. Underhill, *Binding and degradation of hyaluronan by human breast cancer cell lines expressing different forms of CD44: correlation with invasive potential.* J Cell Physiol, 1994. **160**(2): p. 275-86.

45. Ganesh, S., A.K. Iyer, D.V. Morrissey, and M.M. Amiji, *Hyaluronic acid based self-assembling nanosystems for CD44 target mediated siRNA delivery to solid tumors.* Biomaterials, 2013. **34**(13): p. 3489-502.

46. Hiscox, S., B. Baruha, C. Smith, R. Bellerby, L. Goddard, N. Jordan, Z. Poghosyan, R.I. Nicholson, P. Barrett-Lee, and J. Gee, *Overexpression of CD44 accompanies acquired tamoxifen resistance in MCF7 cells and augments their sensitivity to the stromal factors, heregulin and hyaluronan.* BMC Cancer, 2012. **12**: p. 458.

47. Misra, S., P. Heldin, V.C. Hascall, N.K. Karamanos, S.S. Skandalis, R.R. Markwald, and S. Ghatak, *Hyaluronan-CD44 interactions as potential targets for cancer therapy.* Febs j, 2011. **278**(9): p. 1429-43.

48. Altintas, I., R. Heukers, R. van der Meel, M. Lacombe, M. Amidi, P.M. van Bergen En Henegouwen, W.E. Hennink, R.M. Schiffelers, and R.J. Kok, *Nanobody-albumin nanoparticles (NANAPs) for the delivery of a multikinase inhibitor 17864 to EGFR overexpressing tumor cells.* J Control Release, 2013. **165**(2): p. 110-8.

49. Graf, N., D.R. Bielenberg, N. Kolishetti, C. Muus, J. Banyard, O.C. Farokhzad, and S.J. Lippard, *alpha(V)beta(3) integrin-targeted PLGA-PEG nanoparticles for enhanced anti-tumor efficacy of a Pt(IV) prodrug.* ACS Nano, 2012. **6**(5): p. 4530-9.

50. Shen, M., Y. Huang, L. Han, J. Qin, X. Fang, J. Wang, and V.C. Yang, *Multifunctional drug delivery system for targeting tumor and its acidic microenvironment.* Journal of Controlled Release, 2012. **161**(3): p. 884-892.

51. Lee, H., K. Lee, and T.G. Park, *Hyaluronic acid-paclitaxel conjugate micelles: synthesis, characterization, and antitumor activity.* Bioconjug Chem, 2008. **19**(6): p. 1319-25.

52. Li, J., M. Huo, J. Wang, J. Zhou, J.M. Mohammad, Y. Zhang, Q. Zhu, A.Y. Waddad, and Q. Zhang, *Redox-sensitive micelles self-assembled from amphiphilic hyaluronic acid-deoxycholic acid conjugates for targeted intracellular delivery of paclitaxel.* Biomaterials, 2012. **33**(7): p. 2310-20.

53. Lee, H., C.H. Ahn, and T.G. Park, *Poly[lactic-co-(glycolic acid)]-grafted hyaluronic acid copolymer micelle nanoparticles for target-specific delivery of doxorubicin.* Macromol Biosci, 2009. **9**(4): p. 336-

42.

54. Liu, Y., J. Sun, W. Cao, J. Yang, H. Lian, X. Li, Y. Sun, Y. Wang, S. Wang, and Z. He, *Dual targeting folate-conjugated hyaluronic acid polymeric micelles for paclitaxel delivery.* Int J Pharm, 2011. **421**(1): p. 160-9.

55. Jin, Y.J., U. Termsarasab, S.H. Ko, J.S. Shim, S. Chong, S.J. Chung, C.K. Shim, H.J. Cho, and D.D. Kim, *Hyaluronic acid derivative-based self-assembled nanoparticles for the treatment of melanoma.* Pharm Res, 2012. **29**(12): p. 3443-54.

56. Cho, H.J., I.S. Yoon, H.Y. Yoon, H. Koo, Y.J. Jin, S.H. Ko, J.S. Shim, K. Kim, I.C. Kwon, and D.D. Kim, *Polyethylene glycol-conjugated hyaluronic acid-ceramide self-assembled nanoparticles for targeted delivery of doxorubicin.* Biomaterials, 2012. **33**(4): p. 1190-200.

57. Cho, H.J., H.Y. Yoon, H. Koo, S.H. Ko, J.S. Shim, J.H. Cho, J.H. Park, K. Kim, I.C. Kwon, and D.D. Kim, *Hyaluronic acid-ceramide-based optical/MR dual imaging nanoprobe for cancer diagnosis.* J Control Release, 2012. **162**(1): p. 111-8.

58. Cho, H.J., H.Y. Yoon, H. Koo, S.H. Ko, J.S. Shim, J.H. Lee, K. Kim, I.C. Kwon, and D.D. Kim, *Self-assembled nanoparticles based on hyaluronic acid-ceramide (HA-CE) and Pluronic(R) for tumor-targeted delivery of docetaxel.* Biomaterials, 2011. **32**(29): p. 7181-90.

59. Park, J.H., H.J. Cho, U. Termsarasab, J.Y. Lee, S.H. Ko, J.S. Shim, I.S. Yoon, and D.D. Kim, *Interconnected hyaluronic acid derivative-based nanoparticles for anticancer drug delivery.* Colloids Surf B

Biointerfaces, 2014. **121**: p. 380-7.

60. Bontha, S., A.V. Kabanov, and T.K. Bronich, *Polymer micelles with cross-linked ionic cores for delivery of anticancer drugs.* J Control Release, 2006. **114**(2): p. 163-74.

61. Li, A., H.P. Luehmann, G. Sun, S. Samarajeewa, J. Zou, S. Zhang, F. Zhang, M.J. Welch, Y. Liu, and K.L. Wooley, *Synthesis and in vivo pharmacokinetic evaluation of degradable shell cross-linked polymer nanoparticles with poly(carboxybetaine) versus poly(ethylene glycol) surface-grafted coatings.* ACS Nano, 2012. **6**(10): p. 8970-82.

62. Shimoda, A., S. Sawada, A. Kano, A. Maruyama, A. Moquin, F.M. Winnik, and K. Akiyoshi, *Dual crosslinked hydrogel nanoparticles by nanogel bottom-up method for sustained-release delivery.* Colloids Surf B Biointerfaces, 2012. **99**: p. 38-44.

63. Park, J.H., J.Y. Lee, U. Termsarasab, I.S. Yoon, S.H. Ko, J.S. Shim, H.J. Cho, and D.D. Kim, *Development of poly(lactic-co-glycolic) acid nanoparticles-embedded hyaluronic acid-ceramide-based nanostructure for tumor-targeted drug delivery.* Int J Pharm, 2014. **473**(1-2): p. 426-33.

64. Graf, N., D.R. Bielenberg, N. Kolishetti, C. Muus, J. Banyard, O.C. Farokhzad, and S.J. Lippard, *α(V)β(3) integrin-targeted PLGA-PEG nanoparticles for enhanced anti-tumor efficacy of a Pt(IV) prodrug.* ACS Nano, 2012. **6**(5): p. 4530-9.

65. Zhou, J., T.R. Patel, M. Fu, J.P. Bertram, and W.M. Saltzman, *Octa-functional PLGA nanoparticles for targeted and efficient siRNA*

delivery to tumors. Biomaterials, 2012. **33**(2): p. 583-91.

66. Kim, Y.H., J. Jeon, S.H. Hong, W.K. Rhim, Y.S. Lee, H. Youn, J.K. Chung, M.C. Lee, D.S. Lee, K.W. Kang, and J.M. Nam, *Tumor targeting and imaging using cyclic RGD-PEGylated gold nanoparticle probes with directly conjugated iodine-125.* Small, 2011. **7**(14): p. 2052-60.

67. Mitchell, N., T.L. Kalber, M.S. Cooper, K. Sunassee, S.L. Chalker, K.P. Shaw, K.L. Ordidge, A. Badar, S.M. Janes, P.J. Blower, M.F. Lythgoe, H.C. Hailes, and A.B. Tabor, *Incorporation of paramagnetic, fluorescent and PET/SPECT contrast agents into liposomes for multimodal imaging.* Biomaterials, 2013. **34**(4): p. 1179-92.

68. Gianella, A., P.A. Jarzyna, V. Mani, S. Ramachandran, C. Calcagno, J. Tang, B. Kann, W.J. Dijk, V.L. Thijssen, A.W. Griffioen, G. Storm, Z.A. Fayad, and W.J. Mulder, *Multifunctional nanoemulsion platform for imaging guided therapy evaluated in experimental cancer.* ACS Nano, 2011. **5**(6): p. 4422-33.

69. Muthu, M.S., S.A. Kulkarni, A. Raju, and S.S. Feng, *Theranostic liposomes of TPGS coating for targeted co-delivery of docetaxel and quantum dots.* Biomaterials, 2012. **33**(12): p. 3494-501.

70. Zhu, H., Y. Li, R. Qiu, L. Shi, W. Wu, and S. Zhou, *Responsive fluorescent Bi(2)O(3)@PVA hybrid nanogels for temperature-sensing, dual-modal imaging, and drug delivery.* Biomaterials, 2012. **33**(10): p. 3058-69.

71. Park, S.I., E.O. Lee, J.W. Kim, Y.J. Kim, S.H. Han, and J.D. Kim,

Polymer-hybridized liposomes anchored with alkyl grafted poly(asparagine). J Colloid Interface Sci, 2011. **364**(1): p. 31-8.

72. Anders, C.K., B. Adamo, O. Karginova, A.M. Deal, S. Rawal, D. Darr, A. Schorzman, C. Santos, R. Bash, T. Kafri, L. Carey, C.R. Miller, C.M. Perou, N. Sharpless, and W.C. Zamboni, *Pharmacokinetics and efficacy of PEGylated liposomal doxorubicin in an intracranial model of breast cancer.* PLoS One, 2013. **8**(5): p. e61359.

73. Shehata, T., K. Ogawara, K. Higaki, and T. Kimura, *Prolongation of residence time of liposome by surface-modification with mixture of hydrophilic polymers.* Int J Pharm, 2008. **359**(1-2): p. 272-9.

74. Torchilin, V.P., T.S. Levchenko, K.R. Whiteman, A.A. Yaroslavov, A.M. Tsatsakis, A.K. Rizos, E.V. Michailova, and M.I. Shtilman, *Amphiphilic poly-N-vinylpyrrolidones: synthesis, properties and liposome surface modification.* Biomaterials, 2001. **22**(22): p. 3035-44.

75. Papisov, M.I., *Theoretical considerations of RES-avoiding liposomes: Molecular mechanics and chemistry of liposome interactions.* Adv Drug Deliv Rev, 1998. **32**(1-2): p. 119-138.

76. Yang, T., F.D. Cui, M.K. Choi, J.W. Cho, S.J. Chung, C.K. Shim, and D.D. Kim, *Enhanced solubility and stability of PEGylated liposomal paclitaxel: in vitro and in vivo evaluation.* Int J Pharm, 2007. **338**(1-2): p. 317-26.

77. Fossheim, S.L., A.K. Fahlvik, J. Klaveness, and R.N. Muller, *Paramagnetic liposomes as MRI contrast agents: influence of*

liposomal physicochemical properties on the in vitro relaxivity. Magn Reson Imaging, 1999. **17**(1): p. 83-9.

78. Nie, Y., L. Ji, H. Ding, L. Xie, L. Li, B. He, Y. Wu, and Z. Gu, *Cholesterol derivatives based charged liposomes for doxorubicin delivery: preparation, in vitro and in vivo characterization.* Theranostics, 2012. **2**(11): p. 1092-103.

79. Haran, G., R. Cohen, L.K. Bar, and Y. Barenholz, *Transmembrane ammonium sulfate gradients in liposomes produce efficient and stable entrapment of amphipathic weak bases.* Biochim Biophys Acta, 1993. **1151**(2): p. 201-15.

80. Yoshioka, H., *Surface modification of haemoglobin-containing liposomes with polyethylene glycol prevents liposome aggregation in blood plasma.* Biomaterials, 1991. **12**(9): p. 861-4.

81. Liu, Z., Y. Jiao, T. Wang, Y. Zhang, and W. Xue, *Interactions between solubilized polymer molecules and blood components.* J Control Release, 2012. **160**(1): p. 14-24.

82. Szoka, F.C., Jr., D. Milholland, and M. Barza, *Effect of lipid composition and liposome size on toxicity and in vitro fungicidal activity of liposome-intercalated amphotericin B.* Antimicrob Agents Chemother, 1987. **31**(3): p. 421-9.

83. Horowitz, A.T., Y. Barenholz, and A.A. Gabizon, *In vitro cytotoxicity of liposome-encapsulated doxorubicin: dependence on liposome composition and drug release.* Biochim Biophys Acta, 1992. **1109**(2): p. 203-9.

84. Bourguignon, L.Y., G. Wong, C. Earle, K. Krueger, and C.C. Spevak, *Hyaluronan-CD44 interaction promotes c-Src-mediated twist signaling, microRNA-10b expression, and RhoA/RhoC up-regulation, leading to Rho-kinase-associated cytoskeleton activation and breast tumor cell invasion.* J Biol Chem, 2010. **285**(47): p. 36721-35.

85. Gabizon, A.A., Y. Barenholz, and M. Bialer, *Prolongation of the circulation time of doxorubicin encapsulated in liposomes containing a polyethylene glycol-derivatized phospholipid: pharmacokinetic studies in rodents and dogs.* Pharm Res, 1993. **10**(5): p. 703-8.

86. Drummond, D.C., O. Meyer, K. Hong, D.B. Kirpotin, and D. Papahadjopoulos, *Optimizing liposomes for delivery of chemotherapeutic agents to solid tumors.* Pharmacol Rev, 1999. **51**(4): p. 691-743.

Table 1 Characterization of DOX-loaded nanoparticles

Composition	Mean diameter (nm)	Polydispersity index	Zeta potential (mV)	Encapsulation efficiency (%)[a]	Drug content (%)[b]
HACE/DOX NP	153.33 ± 1.60	0.15 ± 0.01	-24.61 ± 1.85	46.45 ± 0.54	5.49 ± 0.07
Interconnected HACE/DOX NP	198.97 ± 18.14	0.28 ± 0.01	-11.54 ± 1.74	89.50 ± 2.37	10.06 ± 0.24

Data are presented as mean ± standard deviation (SD) (n = 3).

[a] $Encapsulation\ efficiency\ (\%) = \frac{actual\ amount\ of\ DOX\ in\ NP}{input\ amount\ of\ DOX\ in\ NP} \times 100$

[b] $Drug\ content\ (\%) = \frac{actual\ amount\ of\ DOX\ in\ NP}{amount\ of\ DOX{-}loaded\ NP} \times 100$

Table 2 Characterization of DCT-loaded nanoparticles

Composition	Mean diameter (nm)	Polydispersity index	Zeta potential (mV)	Encapsulation efficiency (%)[a]
DCT/PLGA NP	254.57 ± 8.98	0.10 ± 0.04	-10.50 ± 0.61	67.11 ± 0.89
DCT/PLGA/ HACE NP	286.20 ± 4.35	0.10 ± 0.04	-15.97 ± 1.28	67.04 ± 0.24

Data are presented as mean ± standard deviation (SD) (n = 3).

[a] $Encapsulation\ efficiency\ (\%) = \frac{actual\ amount\ of\ DCT\ in\ formulation}{input\ amount\ of\ DCT\ in\ formulation} \times 100$

Table 3 Composition of nanohybrid liposomal formulations

Composition	F1	F2	F3
Lipoid E100 (mg)	80	80	80
Cholesterol (mg)	20	20	20
HACE (mg)	20	-	20
DOX HCl (mg)	-	20	20
Magnevist (mL)	2	2	2

Table 4 characterization of liposomal formulations

Formulation	Mean diameter (nm)	Polydispersity index	Zeta potential (mV)	Encapsulation efficiency (%)[a]	Drug content (%)[b]
F1	130.07 ± 4.90	0.24 ± 0.01	-27.92 ± 0.37	-	-
F2	124.47 ± 4.00	0.23 ± 0.01	7.09 ± 0.28	55.21 ± 0.82	1.53 ± 0.02
F3	125.43 ± 4.57	0.21 ± 0.02	-14.29 ± 0.43	58.82 ± 0.31	1.63 ± 0.01

Composition

F1 : Blank magnetic nanohybrid liposome

F2 : DOX-loaded magnetic liposome

F3 : DOX-loaded magnetic nanohybrid liposome

Data are presented as mean ± standard deviation (SD) (n = 3).

$$^{a}Encapsulation\ efficiency\ (\%) = \frac{actual\ amount\ of\ DOX\ in\ Formulation}{input\ amount\ of\ DOX\ in\ Formulation} \times 100$$

$$^{b}Drug\ content\ (\%) = \frac{actual\ amount\ of\ DOX\ in\ Formaulation}{amount\ of\ DOX{-}loaded\ formulation} \times 100$$

Table 5 Pharmacokinetic parameters of DOX after intravenous injection in rats at a dose of 3mg/kg

Parameter	DOX solution	F2	F3
AUC (μg·min/mL)	44.86 ± 6.84	5491.31 ± 1226.13[a]	14731.33 ± 3793.55[ab]
Terminal $t_{1/2}$ (min)	96.47 ± 9.79	314.99 ± 62.69[a]	477.77 ± 62.81[ab]
CL (mL/min/kg)	67.97 ± 9.01	0.57 ± 0.16[a]	0.22 ± 0.06[ab]
MRT (min)	17.71 ± 1.73	319.50 ± 37.54[a]	513.81 ± 57.98[ab]
V_{ss} (mL/kg)	1208.35 ± 241.37	182.66 ± 51.20[a]	110.61 ± 32.36[a]

Data are presented as mean ± SD ($n \geq 3$).

[a] $P < 0.05$ compared to DOX solution group.

[b] $P < 0.05$ compared to F2 group.

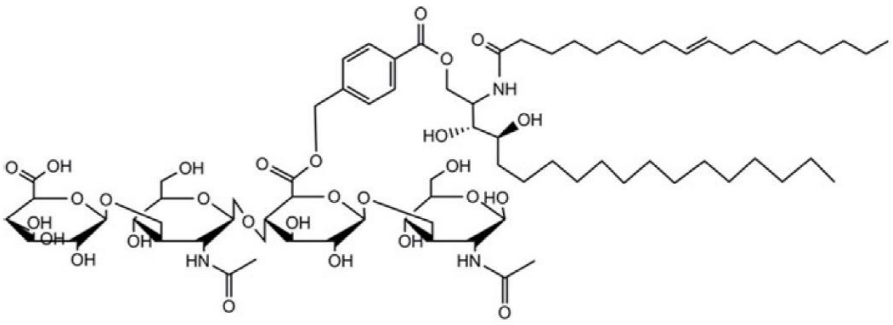

Figure 1 Chemical structure of hyaluronic acid-ceramide

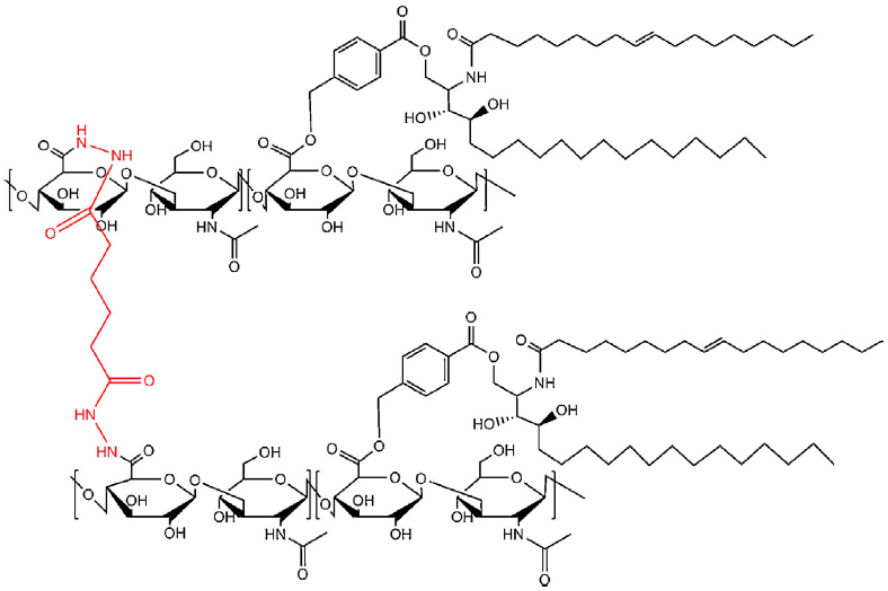

Figure 2 Chemical structure of interconnected hyaluronic acid-ceramide

HACE

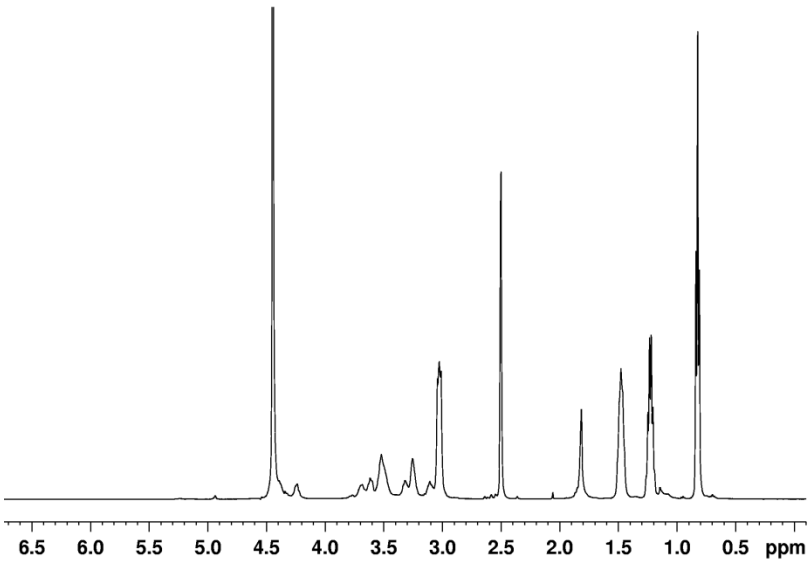

Interconnected HACE

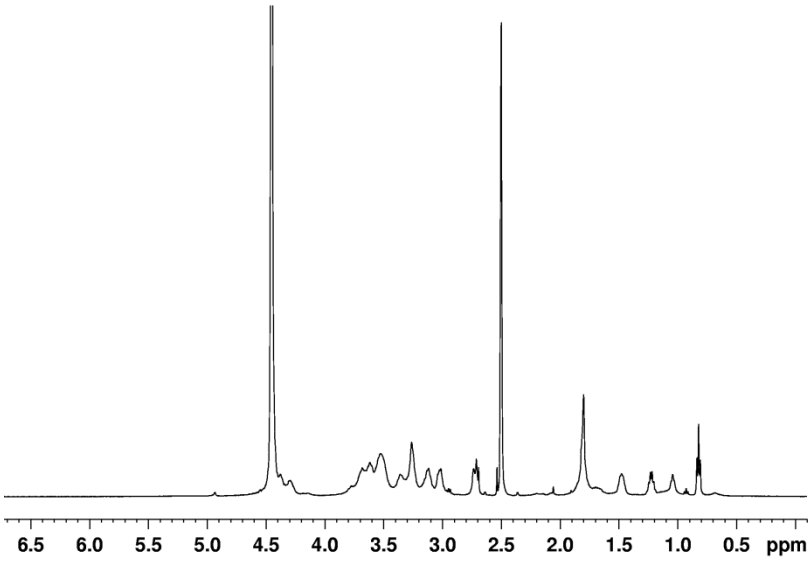

Figure 3 ^{1}H-NMR spectrum of HACE and interconnected HACE, solubilized in d_6-DMSO and D_2O mixture (1:1, v/v)

(a)

HACE/DOX NP **interconnected HACE/DOX NP**

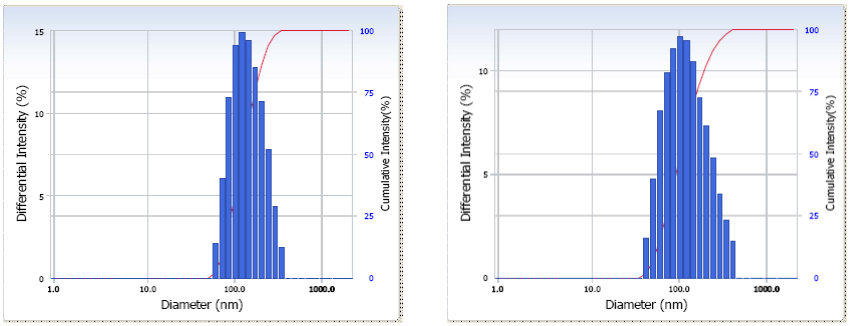

(b)

HACE/DOX NP **interconnected HACE/DOX NP**

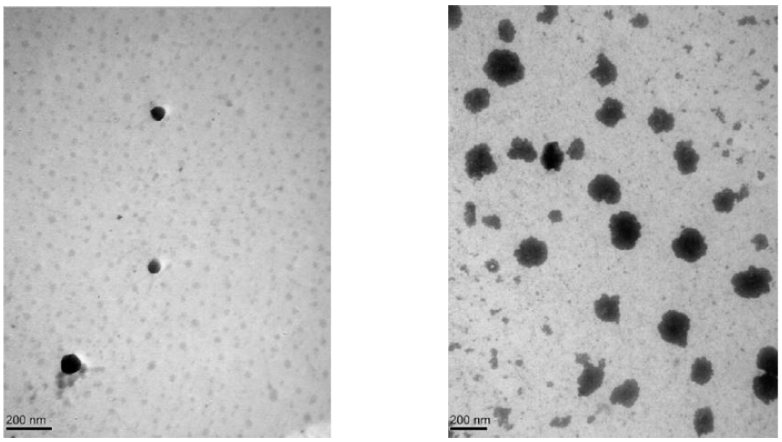

Figure 4 (a) Particle size distribution histograms of DOX-loaded nanoparticles and (b) TEM images of nanoparticles

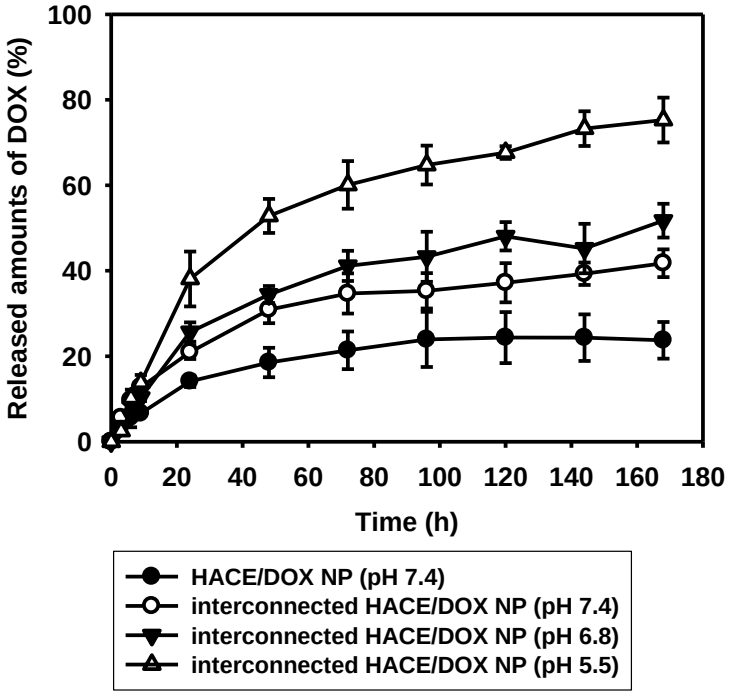

Figure 5 *In vitro* release of DOX from HACE-based nanoparticle formulations measured in different pH condition (pH 5.5, 6.8 and 7.4) (n = 3)

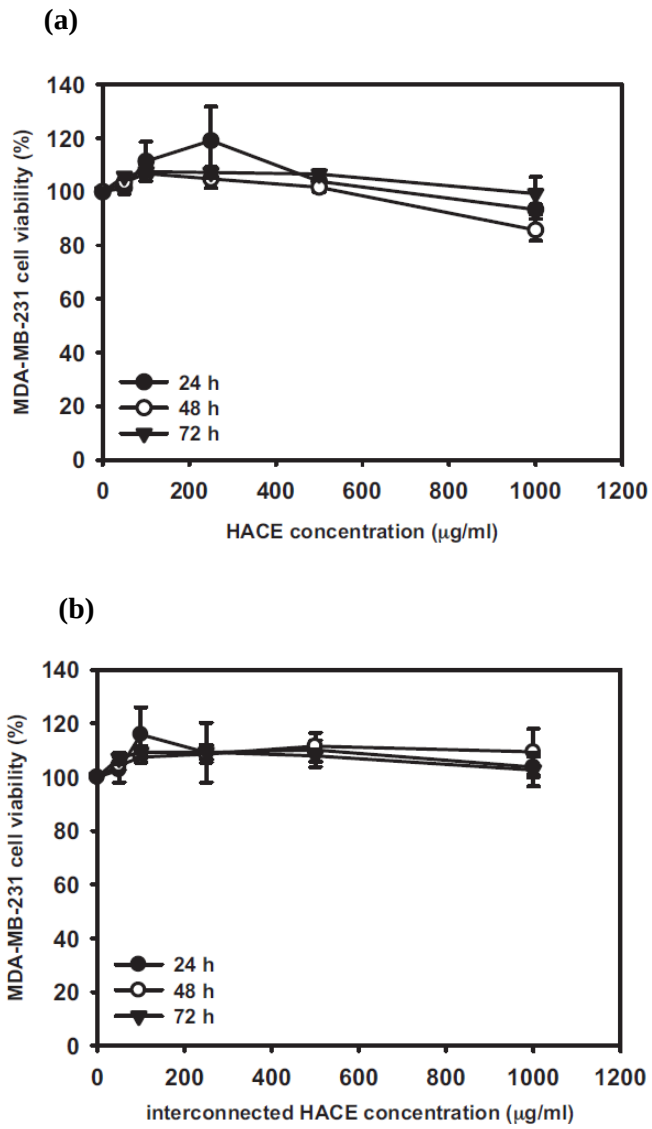

Figure 6 Cytotoxicity test of a (a) HACE and (b) ADH-modified interconnected HACE in the MDA-MB-231 cells (n = 5)

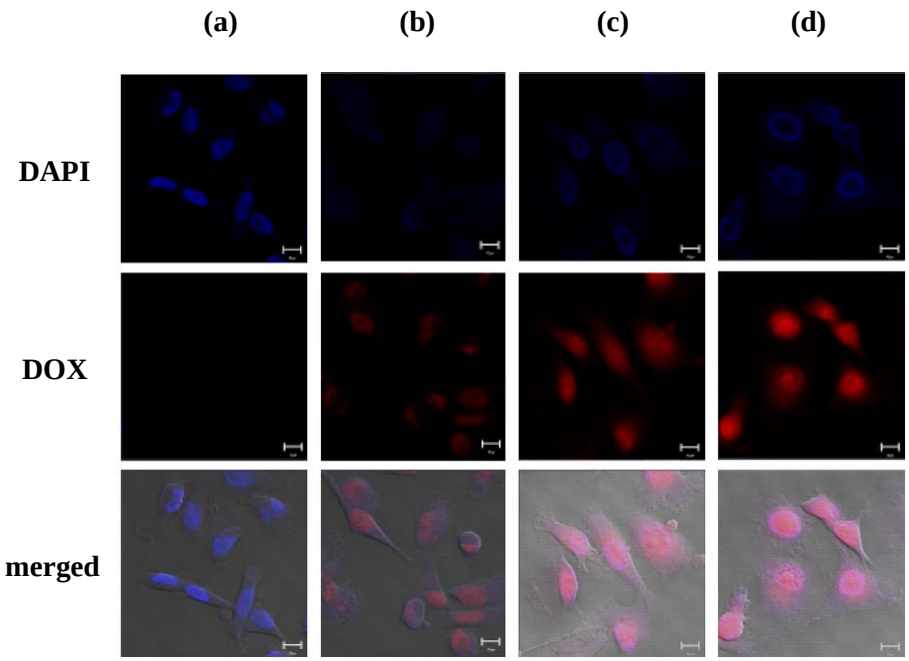

Figure 7 Cellular uptake test of (a) control, (b) DOX solution, (c) DOX-loaded HACE nanoparticles, and (d) DOX-loaded interconnected nanoparticles in MDA-MB-231 cells

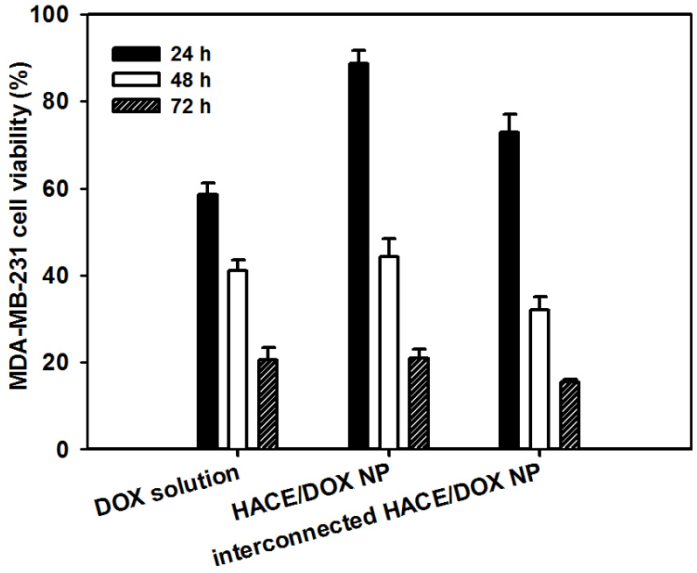

Figure 8 *In vitro* cytotoxicity test of DOX solution, DOX-loaded HACE nanoparticles, and DOX-loaded interconnected nanoparticles in MDA-MB-231 cells (n = 3)

(a)

DCT/PLGA NP **DCT/PLGA/HACE NP**

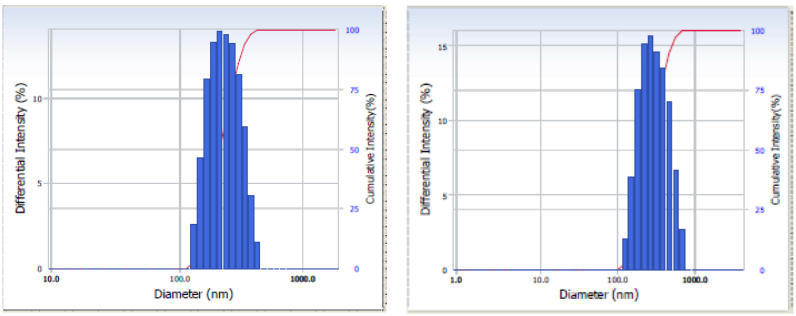

(b)

DCT/PLGA NP **DCT/PLGA/HACE NP**

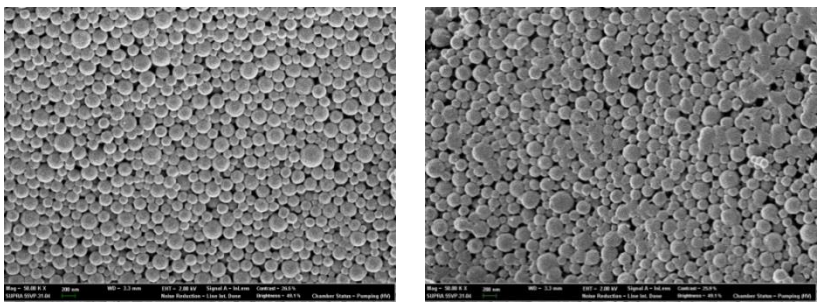

Figure 9 (a) Particle size distribution histograms and (b) SEM images of nanoparticles

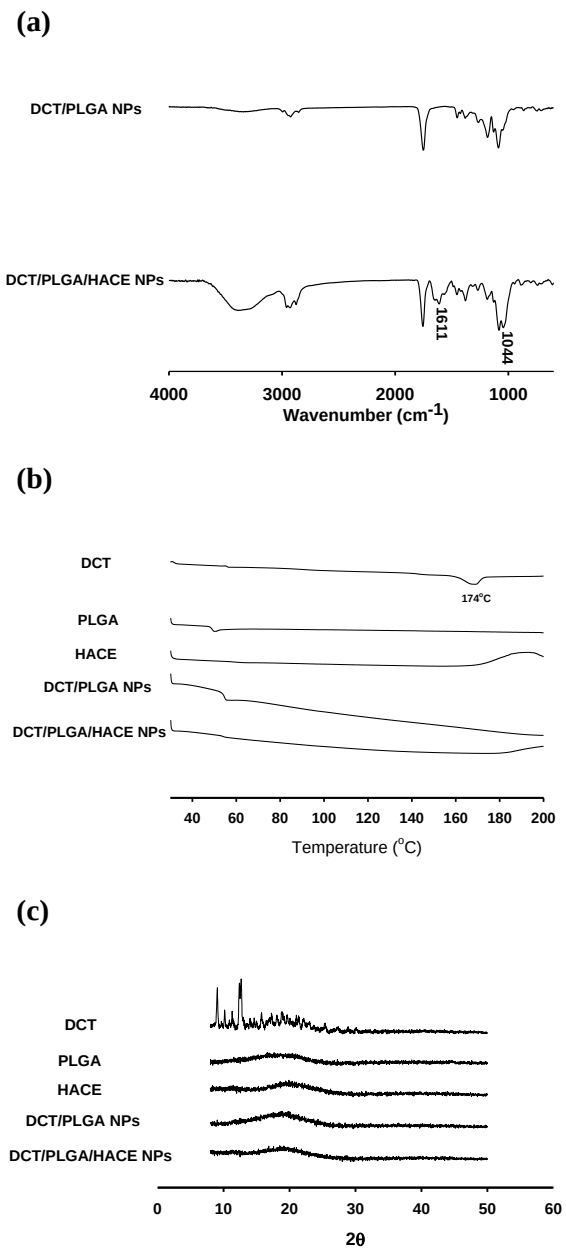

Figure 10 Solid state studies of nanoparticles. (a) FT-IR analysis, (b) DSC analysis and (c) PXRD analysis

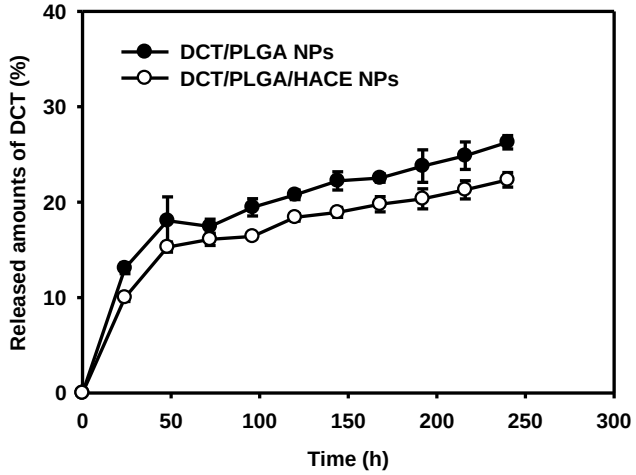

Figure 11 *In vitro* release profiles of DCT/PLGA nanoparticles and DCT/PLGA/HACE nanostructures (n = 3)

(a)

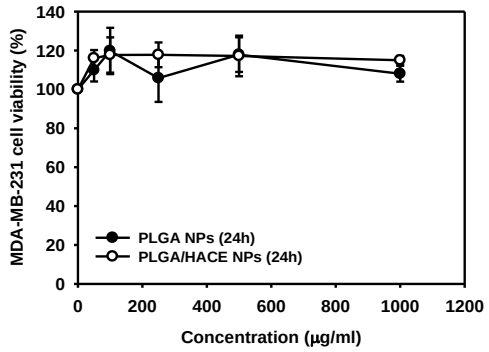

(b)

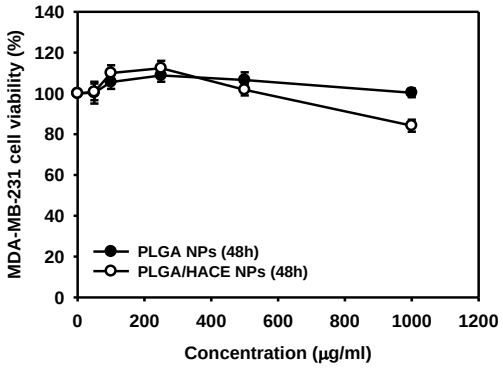

(c)

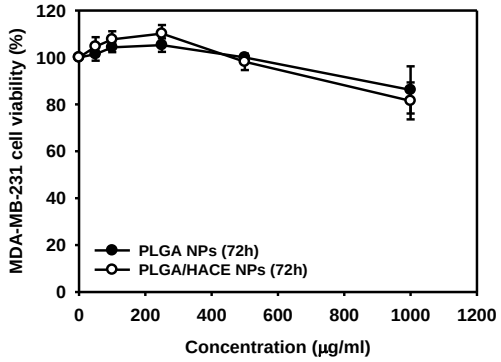

Figure 12 *In vitro* cytotoxicity test of blank PLGA and PLGA/HACE nanoparticles after (a) 24h, (b)48h and (c) 72h of incubation (n = 5)

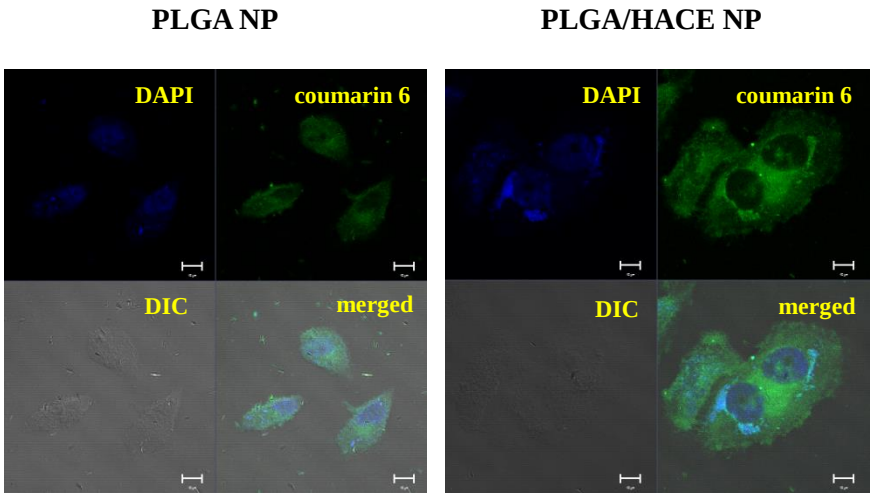

Figure 13 *In vitro* cellular uptake test of coumarin 6-loaded nanoparticles in MDA-MB-231 cells

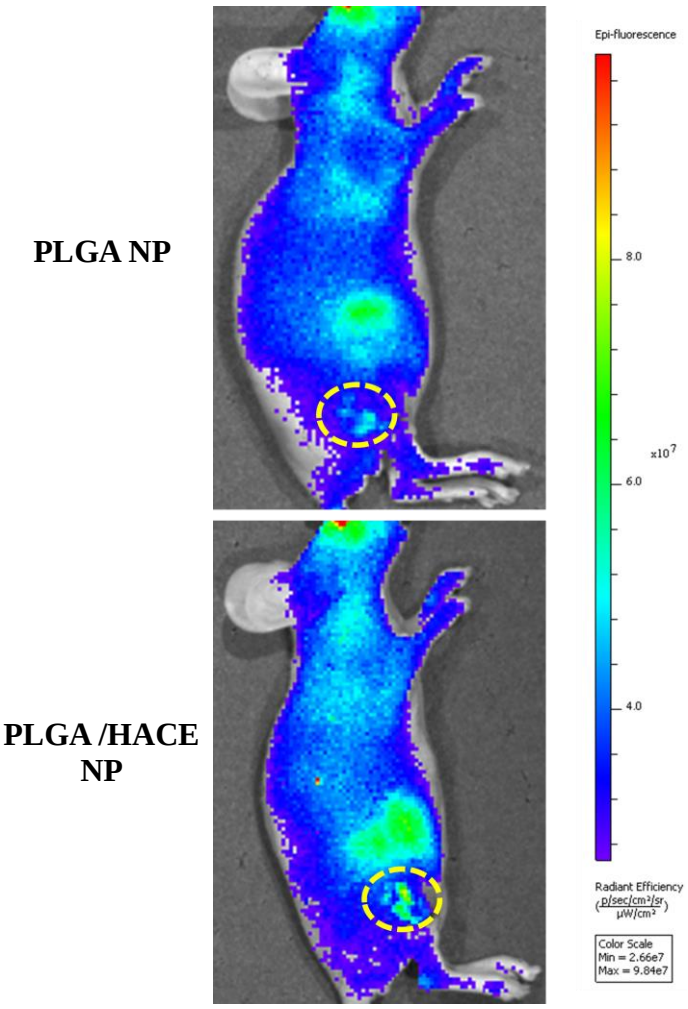

Figure 14 In vivo NIRF imaging in MDA-MB-231 tumor xenografted mouse model after intravenous injection of Cy5.5-conjugated nanoparticles

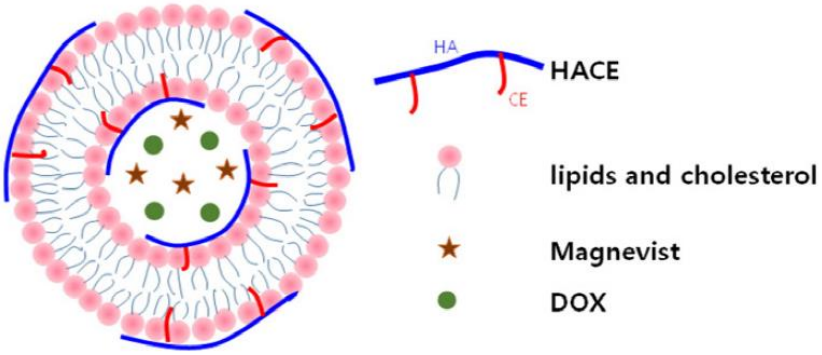

Figure 15 Schematic illustration of MR-visible HACE-coated nanohybrid liposomes containing DOX

F1

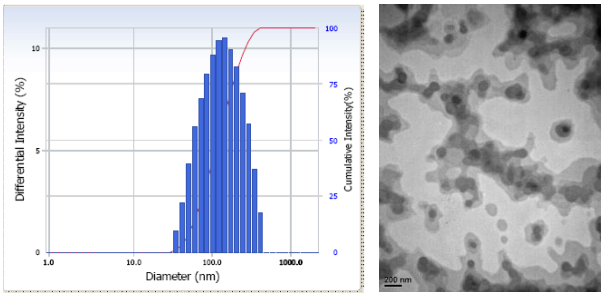

F2

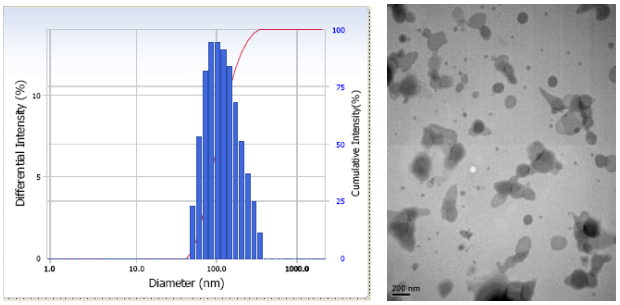

F3

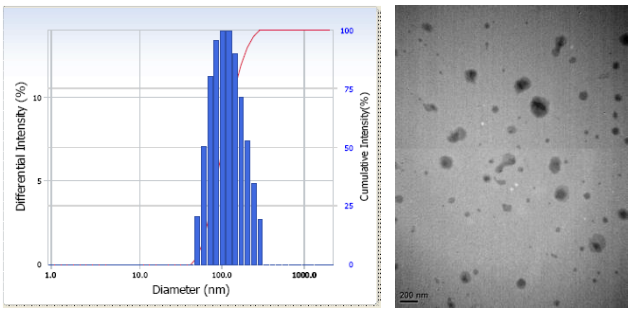

Figure 16 Size distribution histograms (left) and TEM images (right) of liposomal formulations. The scale bar in TEM images represents 200 nm.

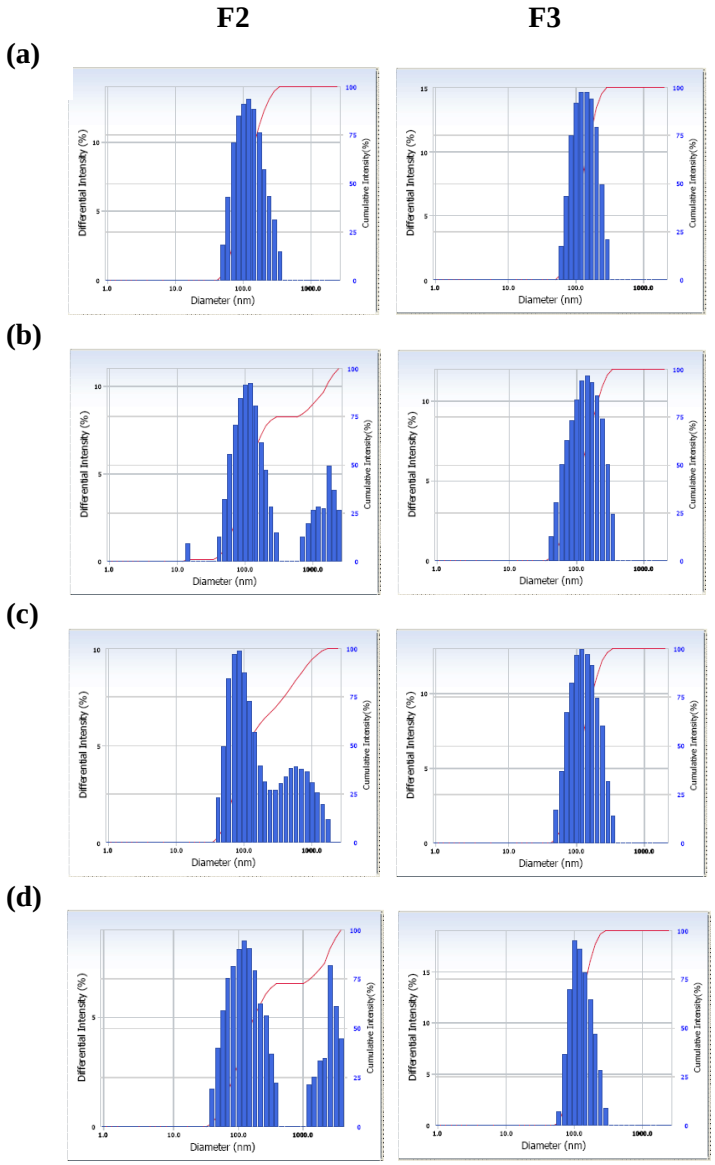

Figure 17 Alteration in size distribution of F2 and F3. Size distribution of each formulation was measured under the following conditions; (a) PBS (pH 7.4), (b) 0 h in 50% FBS solution, (c) 1 h later in 50% FBS solution, and (d) 24 h later in 50% FBS solution.

(a)

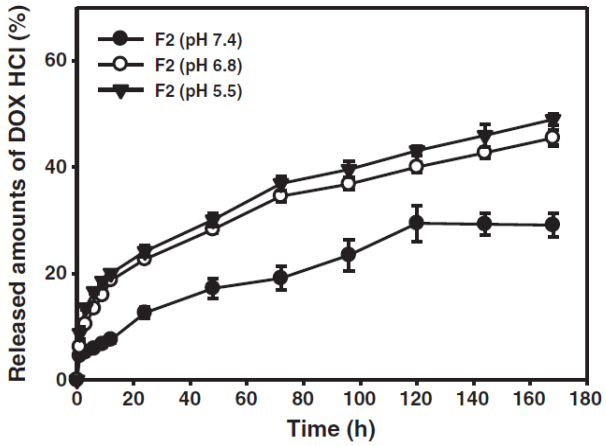

(b)

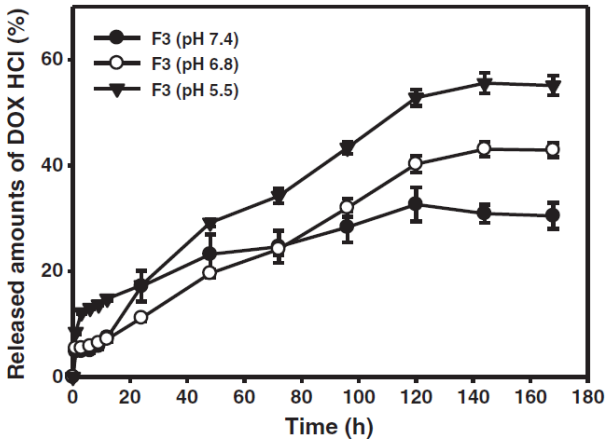

Figure 18 *In vitro* drug release from the developed formulations; F2 (a) and F3 (b). Data are expressed as means ± SD (n = 3)

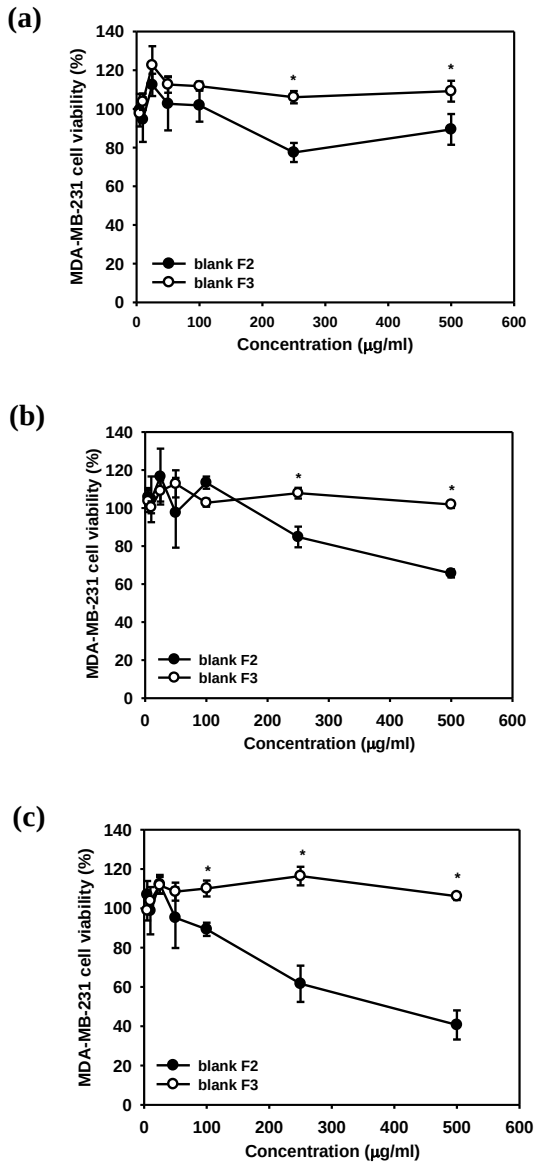

Figure 19 *In vitro* cytotoxicity test of blank F2 and F3 in MDA-MB-231 cells. Cell viability was measured after 24h (a), 48h (b) and 72h (c) of incubation. Data are expressed as means ± SD (n = 4). *P<0.05, compared to that of blank F2.

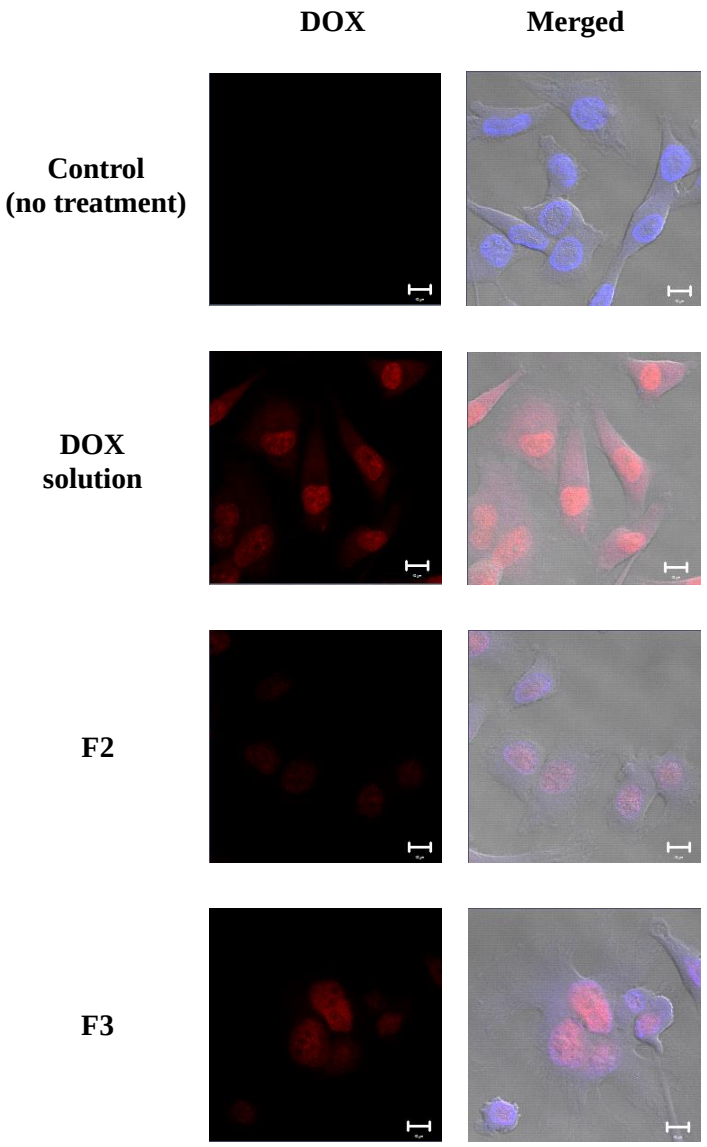

Figure 20 Intracellular distribution profile of DOX solution, F2 and F3 in MDA-MB-231 cells visualized by CLSM after 2 h incubation. (Red and blue colors indicate DOX and DAPI staining, respectively. The length of the scale bar is 10 μm.)

(a)

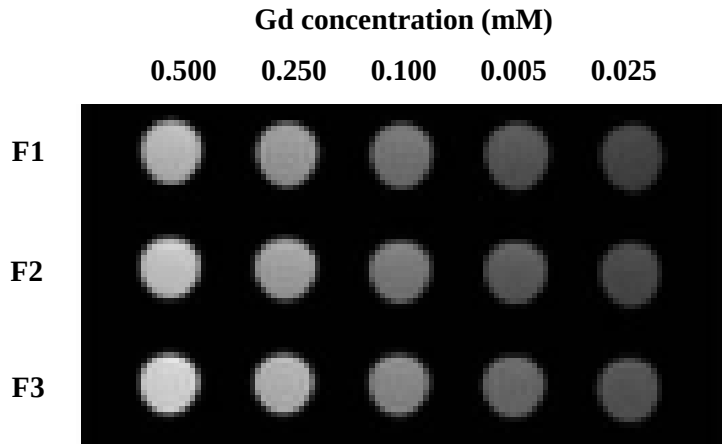

(b)

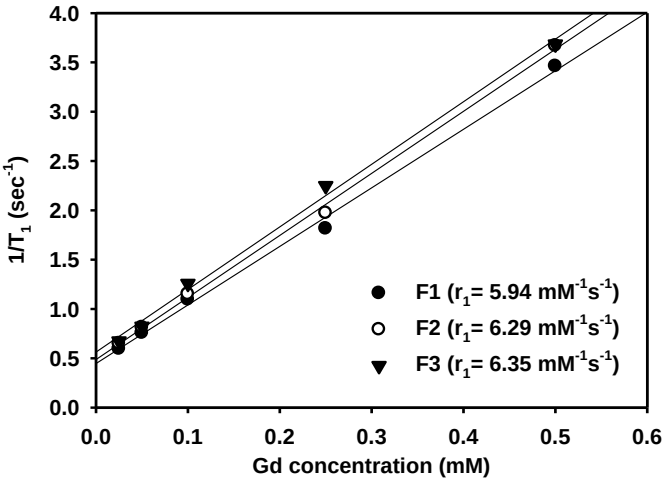

Figure 21 Phantom study of F1, F2 and F3 at 4.7-T. T_1-weighed MRI phantom images at 25-500 μM Gd concentration (a) and the relationship between longitudinal relaxation ($1/T_1$) and Gd concentration.

(a)

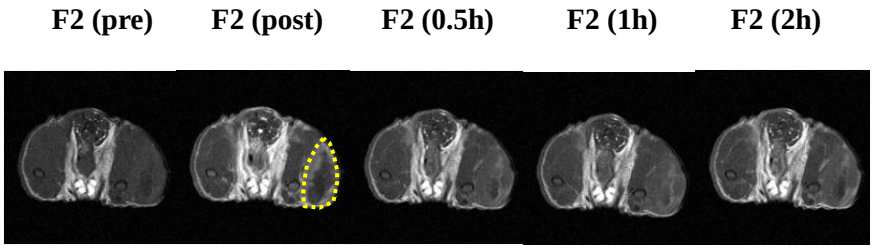

(b)

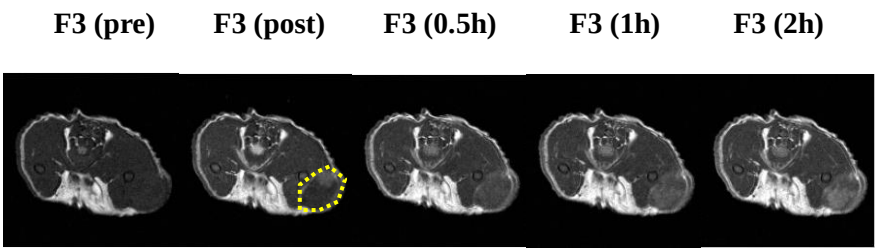

Figure 22 Axial T1-weighed images of MDA-MB-231 tumor-bearing mice before and after the intravenous injection of nanoliposomal formulations (a) F2 and (b) F3 at a dose of 0.1 mmol Gd/kg. The boundary of the tumor region is represented by a yellow dotted line in the post-image (0h).

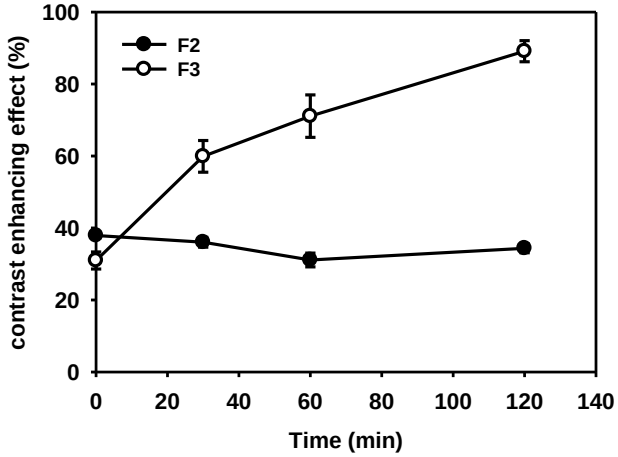

Figure 23 SI change-time profiles (%) in ROI (tumor) of F2 and F3-injected groups. Each point is the mean ± SD (n = 3).

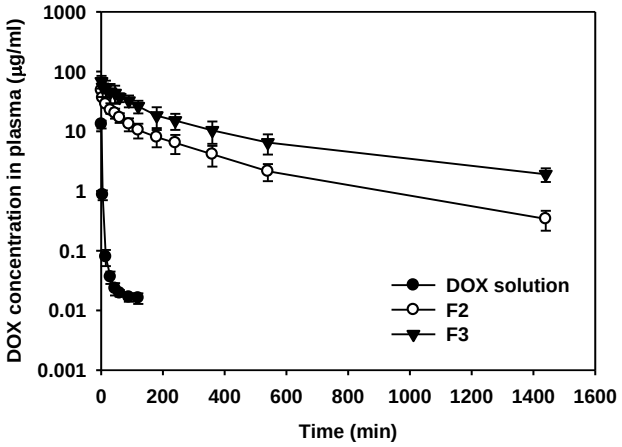

Figure 24 Time-dependent DOX concentration profiles of DOX solution, F2 and F3 in rat plasma. Each point is the mean ± SD ($n \geq 4$).

국문초록

본 연구에서는 항암제의 표적화 전달 및 정확한 암 진단을 위해, 암세포 표적 지향성을 가진 양친매성 고분자인 히알루론산-세라마이드 (HACE)가 적용된 나노리포좀을 제조, 평가하였다. 해당 리포좀 제조에 있어서 독소루비신을 항암제로서 사용하였고, 진단을 위한 자기공명영상 조영제로서 가도펜테틴산-디메글루민이 포함된 마그네비스트 주사제를 사용하였다. 제조 결과, 리포좀의 평균 입자 크기가 120~130 nm 범위이며, 입도분포가 균일하고, 50% 이상의 약물 봉입율을 가지는 것을 확인하였다. HACE 가 사용된 리포좀의 경우 표면 제타전위를 측정, 대조군 리포좀과 비교함으로써 리포좀 표면에 히알루론산 부분이 코팅된 것을 확인하였다. 제조한 리포좀을 대상으로 용출실험을 진행한 결과 두 제제 모두 일주일간 지속적으로 약물이 방출되었고, 낮은 pH 조건에서 용출속도가 증가하였다. 기존 리포좀에 HACE 를 코팅한 결과 혈청 조건에서 안정성이 더 높게 나타났고, 세포를 이용한 안전성 실험에서도 낮은 독성을 보였다. *in vitro* 조건에서 암세포로 약물 적용 시, HACE 코팅된 리포좀의 경우 히알루론산 그룹과 CD44 수용체의 상호작용으로 인해 세포 내 약물 전달이 증가하였다. 암세포가 이식된 누드마우스를 대상으로 리포좀 제제 투여 후 자기공명 이미징 분석 결과, HACE 코팅된 리포좀 적용 시 암 부위에 대한 조영제의 신호 강도가 증가하는 것으로 나타났다. 랫트를 대상으로 약물동태학 실험 시 리포좀 형태로 적용된 경우 용액 형태로 적용할 때보다 현저히 혈중순환이 연장되었고, 혈청 조건에서 안정성이 높았던 HACE 코팅된 리포좀의 경우 기존 리포좀보다 혈중농도를 더 높게 유지하고 소실 속도가 줄어듦을 확인하였다. 위 실험 결과를 미루어볼 때, 리포좀에 HACE 를

적용할 경우 암세포에 대한 표적지향성을 부여하고 제제 자체의 안정성을 증가시킬 수 있어, 항암제의 전달 및 암 진단을 개선시킬 수 있는 것으로 확인되었다.

주요어 : 히알루론산-세라마이드; 나노리포좀; 암 표적화; 약물전달; 자기공명 이미징; 약물동태학적 특성

학번 : 2012-30460